192. F.A. Savin, Yu.V. Morozov, A.V. Borodavkin, V.O. Chekhov, E.I. Budowsky, and N.A. Simukova, Int. J. Quantum. Chem., 16 (1979) 825.
193. S. K. Srivastava and P.C. Mishra, J. Mol. Struct., 65 (1980) 199.

C. Párkányi (Editor) / *Theoretical Organic Chemistry*
Theoretical and Computational Chemistry, Vol. 5

New developments in the analysis of vibrational spectra On the use of adiabatic internal vibrational modes

Dieter Cremer*, J. Andreas Larsson, and Elfi Kraka

Department of Theoretical Chemistry, University of Göteborg, Kemigården 3, S-41296 Göteborg, Sweden

1. INTRODUCTION

Vibrational spectroscopy is an often used tool to identify and characterize a molecule with the help of its vibrational modes. Depending on its geometry, conformation, and electronic structure, each molecule has typical vibrational spectra which are measured with the help of infrared or Raman spectroscopy [1-9]. For example, an infrared band at 1700 cm^{-1} is typical for a carbonyl stretching frequency or one at 700 to 800 cm^{-1} for a CCl bond stretching frequency. In this way, one can draw conclusions from the measured vibrational spectra with regard to the structure of a compound. One can also calculate vibrational frequencies and force constants in the harmonic approximation and these values are often used for the analyses of measured vibrational spectra [10-12]. This is done to identify and verify the structure of molecules generated in the experiment, which will be of particular usefulness if limitations in the experiment do not make any other experimental investigation possible. For example, molecules trapped at low temperatures in a matrix are elegantly investigated by reproducing the measured infrared spectrum by appropriate calculations. In this way a number of labile species have been identified [13-17].

The amount of information contained in a measured vibrational spectrum is exploited to some, but not full extent. For example, vibrational spectra are never used to characterize all bonds of the molecule and to describe its electronic structure and charge distribution in detail. Of course, aspects of such investigations can be found off and on in the literature, however, both quantum chemists and spectroscopists fail to use vibrational spectra on a routine basis as a source of information on bond properties, bond-bond interactions, bond delocalization or other electronic features. Therefore, it is correct to say that the information contained in the vibrational spectra of a molecule is not fully utilized. This has to do with the fact that the analysis of vibrational spectra is always carried out in a way that is far from chemical thinking. The basic instrument in this respect is the normal mode analysis (NMA), which describes the displacements of the atomic nuclei during a molecular vibration in terms of delocalized normal modes [1-6].

A normal mode is composed of the movement of many or even all atoms of a molecule, which is difficult to visualize. Because of this chemists try to simplify the description of a normal mode by focusing on the motions of just few atoms that seem to dominate the normal mode. This requires an appropriate measure that determines which atomic motion is dominant. Attempts in this direction have been made and it is common practice now to associate certain normal modes of a molecule with chemically interesting fragment modes even though this simplification is usually not justified. Hence the basic problem of vibrational spectroscopy is the transformation of the delocalized normal modes, which are difficult to visualize, to chemically more appealing localized modes that can be associated with particular fragments of a molecule.

In this article, we present a new way of analyzing calculated vibrational spectra in terms of internal vibrational modes associated with the internal coordinates used to describe geometry and conformation of a molecule. The internal modes will be determined by solving the Euler-Lagrange equations for molecular fragments ϕ_n being characterized by internal coordinates q_n. An internal mode will be localized in a molecular fragment by describing the rest of the molecule as a collection of massless points that just define molecular geometry. Alternatively, one can consider the new fragment motions as motions that are obtained after relaxing all parts of the vibrating molecule but the fragment under consideration. Because of this property, the internal modes will be called adiabatic internal modes. Once the adiabatic mode vectors are known, adiabatic force constants k_a, adiabatic frequencies ω_a, and adiabatic masses m_a (corresponding to $1/G_{nn}$ of Wilson's G matrix) will be defined. The adiabatic internal modes are independent of the set of internal coordinates used to describe molecular geometry, comply with the symmetry of the molecule, and lead to a clear separation of mass and electronic effects in the vibrational modes of the molecule.

The new modes are perfectly suited to analyze the vibrational spectra of a molecule in terms of internal coordinate modes, to correlate the vibrational spectra of different molecules, and to extract chemically useful information directly from vibrational spectra. It will be shown that adiabatic stretching frequencies and force constants correlate with the corresponding bond lengths and that this can be used to extend Badger's rule from diatomic to polyatomic molecules. The intensities of adiabatic stretching modes lead to effective atomic charges and bond dipole moments. Generalized adiabatic modes will be defined for reacting molecules located somewhere along the reaction path. They will be used to analyze the direction and curvature of the reaction path and, by this, to obtain a better insight into reaction mechanism and reaction dynamics.

2. THE CONCEPT OF LOCALIZED INTERNAL VIBRATIONAL MODES

Chemists have learned to understand geometry and conformation of a molecule in terms of (localized) internal coordinates such as bond lengths, bond angles, and torsional angles. Therefore, it would be chemically useful to discuss

vibrational spectra in terms of bond stretching modes, angle bending modes or torsional modes, which are the localized counterparts of the delocalized normal modes. Each localized mode should be associated with an internal coordinate that describes a molecular fragment of interest. If the normal modes obtained in the NMA of vibrational spectroscopy could be transformed into these internal vibrational modes, then infrared and Raman spectroscopy could provide for each bond a characteristic stretching mode frequency ω_n and a stretching mode force constant k_n that could be used to describe the properties of the bonds of a molecule and that would complement information obtained from direct bond length measurements. Moreover, by determining the bending mode frequencies and force constants of a molecule a direct insight into bond-bond interactions would be provided by vibrational spectroscopy. One could systematically investigate all two-atom, three-atom, four-atom, etc. units of a molecule and, in this way, obtain a detailed description on bonding and electronic structure of a molecule by just using data obtained from vibrational spectroscopy. In this way, vibrational spectroscopy would become a major source of information on molecules, which it is not at the present time.

Of course, one could say that this information can be gained directly from a molecular geometry determination that provides all bond lengths, bond angles, and torsional angles. However, there are several reasons why a description of bonding and other electronic features of a molecule with the help of its vibrational modes should be of advantage. Apart from the fact that it is often easier to measure a vibrational spectrum than to carry out a geometry determination by microwave, electron diffraction or X-ray methods, there is also the reason that the information derived from the vibrational modes has a different quality than that derived from measured bond lengths, bond angles, and dihedral angles. The value of a bond length depends primarily on the accumulation of electron density in the bonding region. It is not very sensitive with regard to the environment of a bond, i.e. the nature of the atoms and groups attached to the bond in question or the electronic characteristics of neighboring bonds. A bond stretching motion, on the other hand, is clearly influenced by the bond environment and, therefore, the internal stretching frequency should reflect not only the amount of electron density accumulated in the bonding region, but also the bulk and electronic nature of the atoms and groups attached to the bond in question. Hence, the internal stretching frequencies and force constants should be a better measure of the strength of the bonds of a molecule than the measured bond lengths.

The information on the various bonds in a molecule should be hidden somewhere in infrared and Raman spectra and it is only a question how to unravel it from experimentally obtained or calculated vibrational spectra. To obtain this information, one has to specify exactly what kind of internal vibrational mode is needed [18-23]:

An internal mode should be fully characterized by only one internal coordinate q_n. The internal coordinate q_n should be the parameter that leads the internal mode and, therefore, it can be called *the leading parameter* of the internal mode [18]. The internal mode should be localized in the fragment ϕ_n of

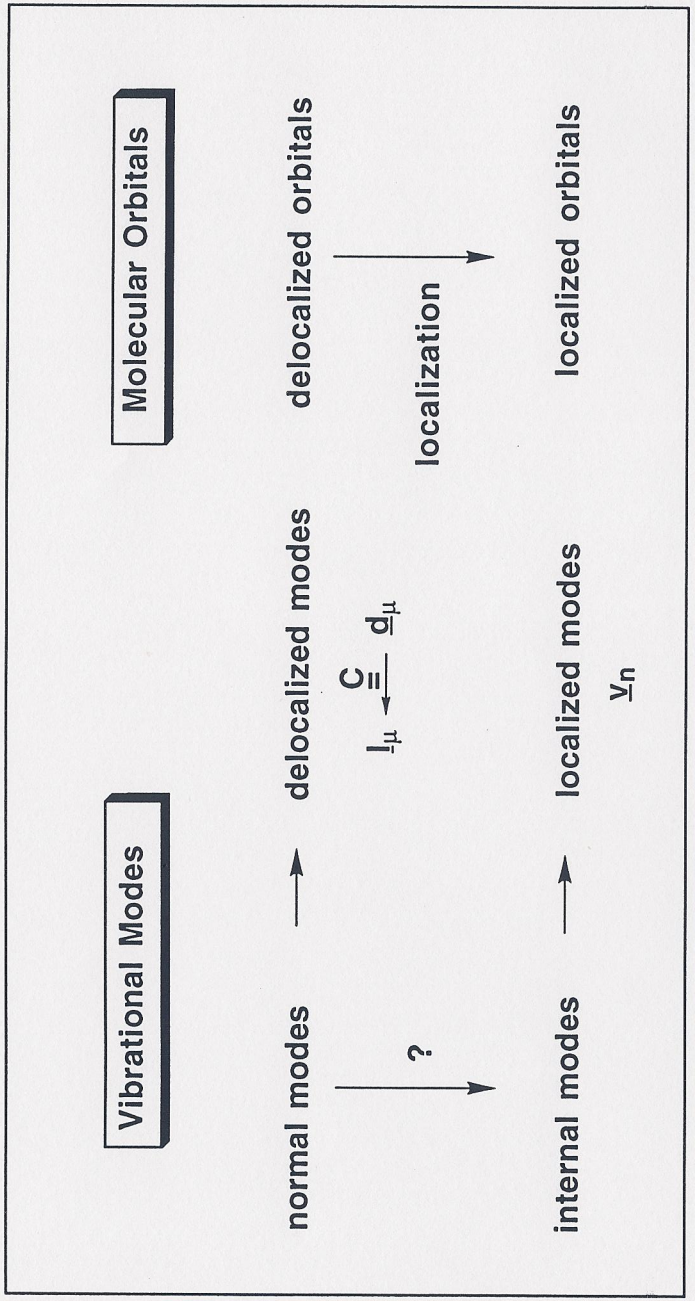

Figure 1. Analogy between delocalized/localized vibrational modes and delocalized/localized molecular orbitals.

the molecule described by the internal coordinate. Of course, this does not necessarily imply that all other atoms are at rest when a fragment is vibrating. On the contrary, to keep all other internal coordinates at their equilibrium values when a particular fragment ϕ_n vibrates, the rest of the molecule has to move with the same frequency than the molecular fragment ϕ_n. However, this is not a contradiction since the motion is still localized in the bond under consideration.

Normal modes are orthogonal to each other and one advantage of this property is that the force constant matrix associated with the normal modes can be given in a diagonal form. Internal modes will no longer be orthogonal, which means that the force constant matrix has no longer a diagonal form. In a way, if the vibrational modes of a molecule are expressed in a form which is closer to chemical thinking, some of these mathematical properties are lost. However, once internal vibrational modes are defined it should be possible to convert back to normal modes and express the latter in terms of internal modes so that it becomes clear to which extent it is justified to interpret normal modes as fragment modes.

An analogy to molecular orbital (MO) theory may help to clarify further what is needed. Chemists prefer to discuss chemical problems in terms of localized MOs rather than in terms of (canonical) delocalized MOs resulting from Hartree-Fock (HF) based quantum chemical calculations. The localized MOs are obtained from the delocalized ones by a transformation ("localization"), which in most cases yields MOs directly related to the bonds of a molecule. The same should be true with regard to localized modes associated with a particular internal coordinate q. The question is only: How can we transform from delocalized normal modes to localized internal modes? To answer this question we will first summarize the basic theory of vibrational spectroscopy.

3. THE BASIC EQUATIONS OF VIBRATIONAL SPECTROSCOPY

The potential energy function V(x) of a molecule with K atoms describes the increase in energy upon a displacement of the atomic nuclei from their equilibrium positions by a Cartesian displacement vector $\mathbf{x} = (x_1, y_1, z_1, \ldots, x_K, y_K, z_K)^+$. Expanding the potential energy in a Taylor series and neglecting all higher order terms one obtains for V(x) expression (1) [1-6]:

$$V(\mathbf{x}) = \frac{1}{2}\mathbf{x}^+\mathbf{f}\mathbf{x} \qquad (1)$$

where **f** is the force constant (Hessian) matrix expressed in Cartesian coordinates at the equilibrium geometry $\mathbf{x}_0 = \mathbf{0}$ because **x** represents the displacements from the equilibrium geometry. The kinetic energy $T(\dot{\mathbf{x}})$ of a vibrating molecule is given by Eq. (2)

$$T(\dot{\mathbf{x}}) = \frac{1}{2}\dot{\mathbf{x}}^+\mathbf{M}\dot{\mathbf{x}} \qquad (2)$$

where **M** is the mass matrix. With Eqs. (1) and (2), the Lagrangian $\mathcal{L}$ of the molecule becomes

$$\mathcal{L}(\mathbf{x},\dot{\mathbf{x}}) = T(\dot{\mathbf{x}}) - V(\mathbf{x}) \tag{3}$$

and the dynamics of the nuclei of the molecule can be determined by solving the Euler-Lagrange equations (4)

$$\frac{d}{dt}\frac{\partial \mathcal{L}(\mathbf{x},\dot{\mathbf{x}})}{\partial \dot{x}_i} - \frac{\partial \mathcal{L}(\mathbf{x},\dot{\mathbf{x}})}{\partial x_i} = 0, \quad i = 1,\ldots,3K \tag{4}$$

The solutions of (4) take the form of (5) [1-6]:

$$\mathbf{x} = \mathbf{l}_\mu Q_\mu \tag{5}$$

where Q_μ is a normal coordinate, which oscillates with the frequency ω_μ according to (6)

$$Q_\mu(t) = a\cos(\omega_\mu t) + b\sin(\omega_\mu t) \tag{6}$$

Inserting (5) and (6) into (4) leads to the basic equation of vibrational spectroscopy [1-6]:

$$\mathbf{f}\,\mathbf{l}_\mu = \omega_\mu^2\,\mathbf{M}\,\mathbf{l}_\mu, \quad \mu = 1,\ldots,N_{vib} \tag{7}$$

which is used to calculate the N_{vib} = 3K-L normal mode frequencies of a K-atomic molecule where L = 5 or 6 gives the number of zero eigenvalues in (7) resulting from translations and rotations of the molecule.

In Eq. (7), the normal mode vectors are expressed in Cartesian coordinate space. However, it is much more useful to express the motions of a molecule in internal coordinate space using N internal coordinates collected in a column vector $\mathbf{q} = (q_1, \ldots, q_N)^+$. Changes in bond lengths, bond angles, and dihedral angles can be used as convenient internal coordinates. To specify the positions of all nuclei in Cartesian space, an additional set of L external coordinates has to be given. The external coordinates are arranged in a column vector $\mathbf{e} = (e_1, \ldots, e_L)^+$. Transformation from internal to Cartesian coordinates is given by Eq.(8) [24]:

$$x_i = \sum_{m=1}^{N} C_{im} q_m + \sum_{\alpha=1}^{L} C_{0,i\alpha} e_\alpha \tag{8}$$

where C_{im} is an element of the (3K,N)-rectangular matrix **C** with column vectors $\mathbf{c}_m$:

$$\mathbf{C} = \mathbf{M}^{-1}\mathbf{B}^+\mathbf{G}^{-1} \tag{9}$$

and matrix $\mathbf{C}_0$ has been defined by Neto [24]. Wilson's **G**-matrix [1] is given by

$$\mathbf{G} = \mathbf{B}\mathbf{M}^{-1}\mathbf{B}^+ \tag{10}$$

and the elements of the **B** matrix are defined by

$$q_n = \sum_{i=1}^{3K} B_{ni} x_i \tag{11}$$

$$B_{ni} = \left(\frac{\partial q_n(\mathbf{x})}{\partial x_i}\right)_{\mathbf{x}=\mathbf{x}_0} \tag{12}$$

with $\mathbf{x}_0$ denoting the equilibrium geometry of the molecule.

Note that

$$\mathbf{B}\mathbf{C} = \mathbf{B}\mathbf{M}^{-1}\mathbf{B}^+\mathbf{G}^{-1} = \mathbf{G}\mathbf{G}^{-1} = \mathbf{I} \tag{13}$$

and

$$\mathbf{B}\mathbf{C}_0 = \mathbf{0}. \tag{14}$$

Generally, internal and external coordinates couple in the kinetic energy term, however they can be decoupled by inserting (8) into (3) and using (14), which leads to

$$\mathcal{L} = \mathcal{L}_{int} + \mathcal{L}_{ext} \tag{15}$$

where $\mathcal{L}_{ext}$ depends on external coordinates and, accordingly, is not relevant for the vibrational problem. The quantity $\mathcal{L}_{int}$ determines the time dependence of the internal coordinates and is given by

$$\mathcal{L}_{int}(\mathbf{q},\dot{\mathbf{q}}) = \frac{1}{2}\dot{\mathbf{q}}^+\mathbf{G}^{-1}\dot{\mathbf{q}} - \frac{1}{2}\mathbf{q}^+\mathbf{F}\mathbf{q} \tag{16}$$

where **F** is the N x N-dimensional force constant matrix expressed in internal coordinate space :

$$F_{nm} = \mathbf{c}_n^+\,\mathbf{f}\,\mathbf{c}_m \tag{17}$$

Solving the Euler-Lagrange equation (18)

$$p_m = \frac{\partial \mathcal{L}_{int}(q,\dot{q})}{\partial \dot{q}_m} \qquad (18a)$$

$$\frac{d}{dt} p_m = \frac{\partial \mathcal{L}_{int}(q,\dot{q})}{\partial q_m} \qquad (18b)$$

$m = 1,\ldots,N$

(p_m is the generalized momentum) leads to Wilson's GF formalism for determining vibrational frequencies ω_μ [1]:

$$\mathbf{F}\mathbf{d}_\mu = \omega_\mu^2 \mathbf{G}^{-1}\mathbf{d}_\mu. \qquad (19)$$

$$\omega_\mu^2 = \frac{\mathbf{d}_\mu^+ \mathbf{F}\,\mathbf{d}_\mu}{\mathbf{d}_\mu^+ \mathbf{G}^{-1}\,\mathbf{d}_\mu}. \qquad (20)$$

Vector $\mathbf{d}_\mu$ represents the normal mode μ in internal coordinate space. It can be transformed to Cartesian coordinate space according to Eq. (21):

$$\mathbf{l}_\mu = \mathbf{C}\,\mathbf{d}_\mu \qquad (21)$$

4. PREVIOUS ATTEMPTS OF DEFINING INTERNAL VIBRATIONAL MODES

The column vectors of C, $\mathbf{c}_n$, can be chosen to represent the internal displacement vectors $\mathbf{v}_n$:

$$\mathbf{v}_n = \mathbf{c}_n \qquad (22)$$

for a given internal coordinate q_n and n = 1, ..., N_{vib}.

The "c-vectors" are implicitly used when expressing normal vibrational modes in terms of internal coordinates or when applying the potential energy distribution (PED) analysis to describe vibrational modes [25-27]. However, they have never been used explicitly to define internal modes of a molecule in the sense of Eq. (22). Since c-vectors are associated with internal coordinates q_n, and each of the latter describes a molecular fragment ϕ_n, they seem to be the natural choice for internal modes. However, it has been shown that $\mathbf{v}_n = \mathbf{c}_n$ is not a satisfactory choice of an internal vibration [19].

One often assumes that certain normal modes and their associated normal mode frequencies represent internal modes and internal mode frequencies (e.g., a normal mode frequency of 1700 cm^{-1} of a ketone as the C=O stretching mode frequency) [1-9]. If a normal mode vector $\mathbf{l}_\mu$ is largely localized in the molecular fragment ϕ_n, then the normal mode frequency ω_μ will be similar to the characteristic fragment frequency $\omega(\phi_n) = \omega_n$. It is one of the major goals of vibrational spectroscopy to determine fragment frequencies ω_n, which can be used to identify functional groups in a molecule to be investigated by vibrational spectroscopy [1-9]. The existence of such frequencies simply results from the fact that functional groups largely retain their properties within different molecular environments. This, in turn, indicates that bonding and electron density distribution of a functional group are largely unaffected by the rest of the molecule and that group characteristic parameters such as internal mode frequency and internal mode force constant are appropriate to describe bonding and electron density distribution of a particular group.

However, using Eq. (21) it is easy to show that such an assumption is strictly valid only for the case where

$$(\mathbf{d}_\mu)_n = \delta_{n\mu} \qquad (23)$$

($\delta_{n\mu}$: Kronecker delta) since this leads to

$$\mathbf{l}_\mu = \mathbf{c}_n \qquad (24)$$

where it is assumed that $\mu = n$. However, even if displacements along vectors $\mathbf{c}_n$ and $\mathbf{c}_m$ do not couple thus leading to a diagonal F matrix with $F_{nm} = 0$ (see Eq. 17, no electronic coupling), there is always mass coupling between the c-vectors because the G matrix is non-diagonal, which according to Eq. (19) leads to $d_{n\mu} \neq \delta_{n\mu}$ and $\mathbf{l}_\mu \neq \mathbf{c}_n$. Nevertheless, most vibrational spectroscopists will assume a more diagonal character of the G matrix if there is a large mass difference between the atoms participating in the molecular motions. In some way, the assumptions made in Eqs. (23) and (24) provide the only basis for an experimentalist to discuss measured frequencies in terms of internal mode frequencies.

Hence, both the choice of c-vectors as internal mode vectors $\mathbf{v}_n$ and the typical assumption $\mathbf{l}_\mu = \mathbf{c}_n$ are not suited to provide an analysis of vibrational spectra in terms of internal modes [18,19]. Therefore, in the next section we will discuss a different approach that is based on a physically reasonable definition of internal modes.

5. DEFINITION OF ADIABATIC INTERNAL MODES

To obtain reasonable internal modes one has to consider that mass coupling prevents the vibrational modes to be localized in a particular molecular fragment. Hence, on has to eliminate mass coupling by an appropriate redefinition of the Euler-Lagrange equations. This is done by simply assuming that in Eqs. (4) all masses but the ones which belong to the atoms of fragment ϕ_n are zero [18]. With this assumption, the equations of motion (4) will lead to a pure internal vibration of fragment ϕ_n. Such an internal vibration expressed in Cartesian coordinate space is of little use for a chemist, who prefers to think in terms of internal coordinates rather than Cartesian coordinates. However, since

$m_i = 0$ ($i \in \phi_m$ with $m \neq n$) implies that the associated generalized momentum p_i is also equal to zero, one can extend the assumption that all atoms not belonging to ϕ_n are massless points just describing the molecular geometry and apply it to internal parameters by assuming that all internal parameters q_m ($m \neq n$) are associated with the generalized momentum $p_m = 0$. With this assumption, the Euler-Lagrange equations (18) take the form of (25) and (26) [18]:

$$p_n = \frac{\partial \mathcal{L}(q,\dot{q})}{\partial \dot{q}_n} \neq 0 \qquad (25a)$$

$$p_m = \frac{\partial \mathcal{L}(\mathbf{q},\dot{\mathbf{q}})}{\partial \dot{q}_m} = 0 \quad \forall m,\ m \neq n \qquad (25b)$$

$$\dot{p}_n = \frac{\partial V}{\partial q_n} \qquad (26a)$$

$$\dot{p}_m = \frac{\partial V}{\partial q_m} = \mathbf{0} \qquad m \neq n \qquad (26b)$$

Eqs. (26) can be solved by adding Eq. (27):

$$\dot{p}_n = \lambda \qquad (27a)$$

$$\lambda = \frac{\partial V}{\partial q_n} \qquad (27b)$$

Eqs. (26b) and (27b) are used to express all internal coordinates q as functions of λ

$$\begin{aligned} q_1 &= q_1(\lambda) \\ &\cdots\cdots\cdots\cdots \\ q_N &= q_N(\lambda) \end{aligned} \qquad (28)$$

Eq. (28) determines the form of internal vibrations $\mathbf{v}_n$ because it defines one-dimensional subspaces within the full configuration space. The motion in an one-dimensional subspace can be described by vector $\mathbf{v}_n$, which can be found by linearization (e.g. *via* a Taylor expansion at point λ=0) of Eq. (28). If needed, the time dependence of λ can be found using generalized momenta

$$p_n = p_n(\mathbf{q},\dot{\mathbf{q}}) = p_n\left(\lambda,\dot{\lambda}\right) \qquad (29)$$

in connection with Eqs. (27a) and (28). In this way, one obtains an internal vibration $\mathbf{v}_n = \mathbf{a}_n$ for parameter q_n associated with fragment ϕ_n.

A set of equations similar to (27) can be obtained by applying a completely different approach [18]. One can displace parameter q_n from its equilibrium value ($q_n = 0$), keep it frozen and equal to a constant q_n^*. At the same time, all other parameters q_m can relax until the molecular energy attains its minimum. Hence, parameter q_n^* leads the corresponding motion as described by Eq. (30)

$$\mathbf{x}^* = \mathbf{v}_n\, q_n^* \qquad (30)$$

(*leading parameter principle* [18]). For obvious reasons, one can call the vibrations generated by q_n^* as adiabatic vibrations defined by (31):

$$V(\mathbf{q}) = \min \qquad (31a)$$

$$q_n = \text{const} = q_n^*. \qquad (31b)$$

Eq. (31) can be easily solved using the method of Lagrange multipliers:

$$\frac{\partial}{\partial q_m}\left[V(\mathbf{q}) - \lambda\left(q_n - q_n^*\right)\right] = 0 \qquad m = 1,\ldots,N \qquad (32)$$

which leads to Eqs. (33)

$$\lambda = \frac{\partial V}{\partial q_n} \qquad (33a)$$

$$0 = \frac{\partial V}{\partial q_m} \quad \forall m,\ m \neq n \qquad (33b)$$

which are identical with Eqs. (27b) and (26b). Hence, the approximation based on "massless internal parameters q_m" is equivalent to the adiabatic approximation.

In quantum chemical calculations, the vibrational problem is normally described in the harmonic approximation. Assuming that the vibrational problem has been solved, potential energy and each internal parameter q_n can be expressed as function of N_{vib} normal mode coordinates Q_μ, [1-6]

$$V(Q) = \frac{1}{2}\sum_{\mu=1}^{N_{vib}} k_\mu Q_\mu^2 \qquad (34)$$

$$q_n(Q) = \sum_{\mu=1}^{N_{vib}} D_{n\mu} Q_\mu \qquad (35)$$

where matrix $\mathbf{D}$ collects in its columns the normal mode vectors $\mathbf{d}_\mu$ expressed in internal coordinate space (compare with Eqs. 19 and 21). Inserting (34) into (31) and using the method of Lagrange multipliers, one obtains

$$\frac{\partial}{\partial Q_\mu}\left[V(Q)-\lambda\left(q_n(Q)-q_n^*\right)\right]=0 \tag{36}$$

and

$$Q_\mu^{(n)}=\frac{D_{n\mu}}{k_\mu}\lambda\,. \tag{37}$$

The superscript n denotes the solution for internal parameter q_n where

$$q_n(Q)=q_n^* \tag{38}$$

as described above. Using equations (35), (37), and (38), λ can be found as function of q_n^*

$$\lambda=\frac{1}{\sum_{\mu=1}^{N_{vib}}\frac{D_{n\mu}^2}{k_\mu}}q_n^* \tag{39}$$

Inserting Eq. (39) into Eq. (37) leads to the normal coordinates as a function of q_n^*

$$Q_\mu^{(n)}=Q_{\mu n}^0 q_n^*, \tag{40}$$

where $Q_{\mu n}^0$ is a constant defined as

$$Q_{\mu n}^0=\frac{\frac{D_{n\mu}}{k_\mu}}{\sum_{\nu=1}^{N_{vib}}\frac{D_{n\nu}^2}{k_\nu}}. \tag{41}$$

According to Eq. (40), any change in parameter q_n^* leads to a movement of all normal coordinates along the adiabatic vector $\mathbf{a}_n$, the components of which in normal coordinate space are given by

$$(a_n)_\mu=Q_{\mu n}^0. \tag{42}$$

With Eq. (42) it is straightforward to transform adiabatic vectors into the space of Cartesian displacements:

$$(a_n)_i=\sum_{\mu=1}^{N_{vib}}l_{i\mu}(a_n)_\mu \qquad i=1,\ldots,3K \tag{43}$$

where $l_{i\mu}$ is a component of the normal mode l_μ defined in Eq. (21).

6. DEFINITION OF ADIABATIC INTERNAL FORCE CONSTANT, MASS, AND FREQUENCY

Once vector $\mathbf{v}_n$ that determines the movement of the molecule under the influence of parameter q_n^* is known, one can define a force constant, that corresponds to such a motion, by inserting (30) into the expression for the potential energy of the molecule in the harmonic approximation:

$$V(q_n^*)=\frac{1}{2}k_n(q_n^*)^2 \tag{44}$$

where the internal force constant k_n is given by

$$k_n=\mathbf{v}_n^+\mathbf{f}\mathbf{v}_n \tag{45}$$

It has been shown [18] that defining an internal mass M_n associated with the internal vibration $\mathbf{v}_n$ by

$$M_n=\mathbf{v}_n^+\mathbf{M}\mathbf{v}_n. \tag{46}$$

which implies an characteristic fragment frequency Ω_n:

$$\Omega_n^2=\frac{k_n}{M_n} \tag{47}$$

is not a useful choice since all masses of the molecule contribute to the mass M_n, which enters into the definition of Ω_n. In this way, the internal frequency Ω_n becomes sensitive to the environment of molecular fragment ϕ_n. This can lead to nonphysical shifts of internal frequencies as was documented in the literature [19].

Therefore, one has to proceed in a different way to find a typical mass m_n that opposes any change in the internal parameter q_n. In this connection, two conditions should be fulfilled. First, the mass m_n should be extractable from the functional form of the internal coordinate q_n. Secondly, m_n should be directly connected to the vibrational motion $\mathbf{v}_n$ caused by a change in q_n.

To fulfil these two conditions, one has to ask how the atoms of the molecule have to move so that the kinetic energy adopts a minimum and the generalized velocity $\dot{q}_n$ becomes identical with $\dot{q}_n^*$, i.e. the system fulfils Eqs. (48) and (49):

$$T(\dot{\mathbf{x}}) = \frac{1}{2}\,\dot{\mathbf{x}}^+\,\mathbf{M}\,\dot{\mathbf{x}} = \min \tag{48}$$

$$\mathbf{b}_n^+\,\dot{\mathbf{x}} = \mathbf{b}_n^+\,\mathbf{v}_n\,\dot{q}_n^* \tag{49}$$

where vector $\mathbf{b}_n$ corresponds to the nth column of the **B** matrix [1-6] and $\mathbf{b}_n^+\,\mathbf{v}_n\,\dot{q}_n^*$ is the generalized velocity of internal coordinate q_n when the system moves according to Eq. (30). Using the Lagrange multiplier λ and combining (48) and (49), one obtains

$$\frac{\partial}{\partial \dot{x}_i}\left(\frac{1}{2}\dot{\mathbf{x}}^+\mathbf{M}\dot{\mathbf{x}} - \lambda\left(\mathbf{b}_n^+\dot{\mathbf{x}} - \mathbf{b}_n^+\mathbf{v}_n\,\dot{q}_n^*\right)\right) = 0 \tag{50}$$

and

$$\dot{\mathbf{x}} = \mathbf{M}^{-1}\,\mathbf{b}_n\,\lambda\,. \tag{51}$$

By inserting Eq. (51) into Eq. (49), the Lagrange multiplier λ is given by Eq. (52):

$$\lambda = \frac{\mathbf{b}_n^+\,\mathbf{v}_n}{\mathbf{b}_n^+\,\mathbf{M}^{-1}\,\mathbf{b}_n}\,\dot{q}_n^* \tag{52}$$

With Eq. (52), $\dot{\mathbf{x}}$ of (51) can be determined as a function of $\dot{q}_n^*$. In turn, the kinetic energy of (48) can be written according to (53)

$$T(\dot{q}_n^*) = \frac{1}{2}\,m_n\,(\dot{q}_n^*)^2 \tag{53}$$

with the internal mass m_n associated with parameter q_n being given by

$$m_n = \frac{\left(\mathbf{b}_n^+\,\mathbf{v}_n\right)^2}{\mathbf{b}_n^+\,\mathbf{M}^{-1}\,\mathbf{b}_n} \tag{54}$$

The denominator of Eq. (54) can be recognized as element G_{nn} of the **G** matrix.

Once the internal force constant k_n (see Eq. 45) and the internal mass m_n (see Eq. 54) have been derived, the internal frequency ω_n is given by Eq. (55):

$$\omega_n^2 = \frac{\mathbf{v}_n^+\,\mathbf{f}\,\mathbf{v}_n}{\left(\mathbf{b}_n^+\mathbf{v}_n\right)^2\,\dfrac{1}{G_{nn}}} \tag{55}$$

Eq. (55) implies that if internal coordinate q_n represents the change in the bond distance of a diatomic molecular fragment AB caused by AB bond stretching, then $1/G_{nn}$ will be exactly equal to the reduced mass defined by $m_A m_B/(m_A+m_B)$. Furthermore, Eq. (55) reveals that in the general case $1/G_{nn}$ can be taken as the reduced mass associated with internal coordinate q_n, no matter which functional form q_n takes.

The term $(\mathbf{b}_n^+\mathbf{v}_n)^2$ in the denominator of Eq. (55) guarantees proper normalization of vector $\mathbf{v}_n$. It suggests that the force constant k_n should be calculated according to Eq. (56) rather than Eq. (45):

$$k_n = \mathbf{v}_n'^+\,\mathbf{f}\,\mathbf{v}_n' \tag{56}$$

with $\mathbf{v}_n'$ given by

$$\mathbf{v}_n' = \frac{\mathbf{v}_n}{\mathbf{b}_n^+\mathbf{v}_n} \tag{57}$$

This means that in Eq. (30) $\mathbf{v}_n'$ rather than $\mathbf{v}_n$ is used:

$$\mathbf{x}^* = \mathbf{v}_n'\,q_n^* \tag{58}$$

If Eq. (58) is multiplied from the left by $\mathbf{b}_n^+$, then one will obtain $q_n = (\mathbf{b}_n^+\mathbf{v}_n')q_n^*$. Because of Eq. (57) $\mathbf{b}_n^+\mathbf{v}_n' = 1$, which ensures that q_n and q_n^* are the same during an internal vibration. This is of crucial importance for the calculation of internal force constants. If $\mathbf{v}_n = \mathbf{a}_n$, $\mathbf{v}_n$ will be properly normalized in the sense that $\mathbf{b}_n^+\mathbf{a}_n = 1$ (see Eq. 31b). The term $(\mathbf{b}_n^+\mathbf{v}_n)^2$ in the denominator of (55) is important only when q_n is not equal to q_n^*. This is the case for c-vectors calculated with redundant sets of parameters [19].

7. CHARACTERIZATION OF NORMAL MODES IN TERMS OF INTERNAL VIBRATIONAL MODES

In the previous section, we have determined elementary modes of suitable structural units or molecular fragments ϕ_n that are associated with internal coordinates q_n describing these fragments. These so-called internal modes [18,19] play the same role in the understanding of the vibrating molecule as internal coordinates play in the understanding of molecular geometry and conformation, i.e. internal modes add a dynamic part to the static description of molecules with the help of internal coordinates.

The characterization of normal modes in terms of the localized internal modes (CNM analysis) [20] complements the NMA of vibrational spectroscopy and introduces a chemical aspect into vibrational spectroscopy, namely the

description of the dynamic behavior of molecules in terms of the dynamical properties of groups and molecular fragments. For the purpose of the CNM analysis, one has to define an amplitude $A_{n\mu}$, which specifies the contribution of a particular internal mode $\mathbf{v}_n$ to a given delocalized normal mode $\mathbf{l}_\mu$ [20]. Utilizing amplitudes $A_{n\mu}$, one can decompose normal modes in terms of internal modes and, in this way, exactly relate the normal modes of a molecule to its structural units. This clearly facilitates the use of vibrational spectroscopy as a structure determining tool and extends its possible uses within chemistry.

Clearly, the assets of a useful, in itself noncontradictory, and physically based CNM analysis are the internal vibrational motions and their properties as well as the amplitudes that relate internal modes to normal modes. As shown in the previous section, the *adiabatic internal modes* $\mathbf{a}_n$ are the appropriate candidates for internal modes. Adiabatic modes are based on a dynamic principle, they are calculated by solving the Euler-Lagrange equations, they are independent of the composition of the set of internal coordinates to describe a molecule, and they are unique in so far as they provide a strict separation of electronic and mass effects [18,19]. Therefore, they fulfil the first requirement for a physically based CNM analysis.

There are no explicit criteria that help to define a suitable amplitude A needed to describe the contribution of internal modes to normal modes and, then, to judge on the quality of this definition. However, there are properties that are implicitly assumed to be associated with amplitudes A. These can be formulated in the following way [20]:

1) Symmetry equivalent internal modes associated with symmetry equivalent internal coordinates must have the same amplitudes in the case that the normal mode being decomposed is symmetric. (*Symmetry criterion*)

2) The results of the CNM analysis should not change significantly if some internal motions with low amplitudes are changed or deleted in the expansion of the normal modes as it might happen when changing a redundant set of internal parameters into another set. (*Stability of results*) This can be checked by calculating amplitudes $A_{n\mu}$ of the same internal motions associated with the same internal coordinates q_n for a sequence of different parameter sets PSA, PSB, etc. The difference in amplitudes $\Delta A_{n\mu} = |A_{n\mu}(\mathrm{PSA}) - A_{n\mu}(\mathrm{PSB})|$ has to be evaluated for those internal motions covered by all parameter sets and summed over all normal modes $\mathbf{l}_\mu$ to obtain ΔA as a bar spectrum for the internal coordinates q_n considered. The spectrum ΔA-q_n provides a direct insight into the usefulness of the internal mode vectors $\mathbf{v}_n$ and amplitudes $A_{n\mu}$ within the CNM analysis. (*Stability test of A with regard to variations in the parameter set used*)

3) Since it is not possible to directly evaluate the quality of a given definition of $A_{n\mu}$ one has to do this in an indirect way by comparing a normal mode frequency with suitable reference frequencies associated with internal coordinates q_n. It is physically reasonable to expect that if all normal modes $\mathbf{l}_\mu$ are studied for fixed internal modes $\mathbf{v}_n$ (associated with fixed parameters q_n), then the magnitude of amplitudes $A_{n\mu}$ should become the smaller the larger the difference $\Delta\omega_{n\mu}$ between the normal mode frequency ω_μ and the fixed reference frequency ω_n is. Therefore,

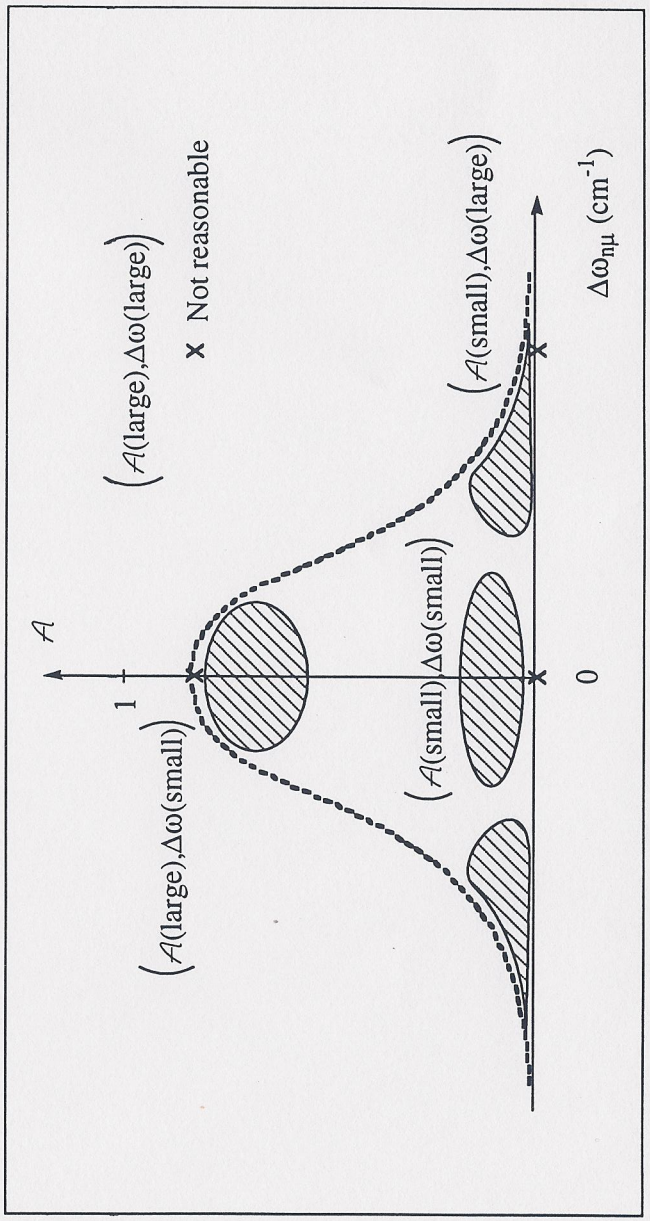

Figure 2. Different possibilities that can occur when plotting amplitudes $A_{n\mu}$ in dependence of the difference $\Delta\omega_{n\mu}$ between normal mode frequencies ω_μ and internal mode frequencies ω_n. The dashed line indicates the enveloping Lorentzian (bell-shaped) curve that can be expected in the case of a physically well-defined amplitude.

the distribution of all amplitudes $A_{n\mu}$ in dependence of differences $\Delta\omega_{n\mu} = \omega_n - \omega_\mu$ should be enveloped by a Lorentzian- (bell-)shaped curve as shown in Figure 2. The scattering of $A_{n\mu}$ in dependence of differences $\Delta\omega_{n\mu}$ outside or inside this enveloping curve provides a direct qualitative impression on the usefulness of the chosen amplitude and its underlying dynamical origin. If there are no amplitudes outside the enveloping curve, one can say that the dynamical origin of the normal mode principle will be fulfilled. (*Dynamical origin of normal mode concept*)

4) While 3) provides a crude qualitative test, its quantification is given by the quantity $h_{n\mu}$

$$h_{n\mu} = A_{n\mu}\,\Delta\omega_{n\mu} \tag{59}$$

which has the dimension of a frequency and can be considered as an uncertainty of the internal mode frequency. It provides a quantitative measurement of the usefulness of amplitude $A_{n\mu}$. In the normal case, the uncertainty $h_{n\mu}$ should have small vanishing values while an accumulation of large $h_{n\mu}$ values indicates deficiencies of amplitudes $A_{n\mu}$. (*Uncertainty test of internal mode frequencies*)

Provided the dynamical origin of the normal mode concept is correctly considered, the amplitude $A_{n\mu}$ will adopt a large value if the frequency difference $\Delta\omega_{\mu n} = \omega_\mu - \omega_n$ is relatively small, which simply means that the internal mode $\mathbf{v}_n$ associated with the internal coordinate q_n dominates the normal mode $\mathbf{l}_\mu$ and that the normal mode frequency ω_μ indicates the presence of the structural unit ϕ_n characterized by q_n and the internal mode frequency ω_μ:

$$A_{n\mu}(\text{large}) \Rightarrow \Delta\omega_{\mu,n}(\text{small}) \tag{60}$$

Relationship (60) is the basis for the empirical assignment of measured frequencies to structural units or fragments of a molecule.

Similarly, if there is a normal mode frequency ω_μ placed far from an internal mode frequency ω_n associated with fragment ϕ_n, then one will not expect a large amplitude since it is unlikely that the internal mode $\mathbf{v}_n$ dominates the normal mode $\mathbf{l}_\mu$.

$$\Delta\omega_{\mu,n}(\text{large}) \Rightarrow A_{n\mu}(\text{small}) \tag{61a}$$

Hence, the case

$$\Delta\omega_{\mu,n}(\text{large}) \Rightarrow A_{n\mu}(\text{large}) \tag{61b}$$

should not occur. Of course, due to strong couplings within the molecule it can happen that, although a normal mode frequency ω_μ possesses a similar value as the internal mode frequency ω_n, normal mode $\mathbf{l}_\mu$ has nothing in common with internal mode $\mathbf{v}_n$. This will be indicated by a low value of amplitude $A_{n\mu}$ according to

$$\Delta\omega_{\mu,n}(\text{small}) \Rightarrow A_{n\mu}(\text{small}) \tag{62}$$

If amplitudes $A_{n\mu}$ are plotted as a function of $\Delta\omega_{\mu n}$, then the distribution of amplitude points should be enveloped by the Lorentzian (bell-shaped) curve of Figure 2 similar to the one describing the line shape of spectroscopic bands [9] since this curve complies with expectations (60) - (62).

8. DEFINITION OF INTERNAL MODE AMPLITUDES A

Any procedure to define an amplitude A must guarantee that normal and internal vibrational modes are related in a physically reasonable way [20]. The internal mode vector $\mathbf{v}_n$ describes how the molecule vibrates when internal coordinate q_n that initiates ("leads") the internal motion is slightly distorted from its equilibrium value. From the NMA, one obtains normal mode vectors l_μ, each of which shows how the atoms of a molecule move when the normal coordinate Q_μ is changed. By comparing the normal mode l_μ with the internal mode $\mathbf{v}_n$ the amplitude $A_{n\mu}$ is obtained that describes l_μ in terms of the vibration of the smaller structural unit ϕ_n represented by displacement vector $\mathbf{v}_n$. Clearly, amplitude $A_{n\mu}$ has to be defined as a function of l_μ and $\mathbf{v}_n$:

$$A_{n\mu} = f\left(\mathbf{l}_\mu, \mathbf{v}_n\right) \tag{63}$$

The internal mode vector $\mathbf{v}_n$ can be defined with the help of the **c**-vectors (Eq. 22) as is implicitly assumed within the PED analysis [25-27]. Alternatively, one can use the adiabatic internal modes $\mathbf{a}_n$ which are led by the associated internal parameters q_n as internal vibrational modes. The latter are preferred since they have a better physical justification than vectors $\mathbf{c}_n$, which should pay off when defining the amplitude $A_{n\mu}$ [18-20].

Once $\mathbf{v}_n$ is chosen, one can compare the normal mode vibration l_μ, with the vibration $\mathbf{v}_n$ of a structural unit ϕ_n according to Eq. (64) [20]

$$A_{n\mu} = \frac{\left(\mathbf{l}_\mu, \mathbf{v}_n\right)^2}{\left(\mathbf{v}_n, \mathbf{v}_n\right)\left(\mathbf{l}_\mu, \mathbf{l}_\mu\right)} \tag{64}$$

where the symbol $A_{n\mu}$ is used to distinguish between a specific definition of A and the general amplitude $A_{n\mu}$. The denominator in (64) accounts for proper normalization and guarantees that $A_{n\mu}$ will adopt values between 0 and 1.

The scalar product $(\mathbf{a},\mathbf{b})$, which appears in the definition of the amplitude $A_{n\mu}$ (Eq. 64), can be defined in the most general way as

$$(\mathbf{a},\mathbf{b}) = \sum_{i,j} a_i O_{ij} b_j \tag{65}$$

where O_{ij} is an element of the metric matrix **O** and a_i and b_j are components of vectors **a** and **b** in Cartesian space. For the metric **O**, there are three natural choices, namely

$$O_{ij} = \delta_{ij} \tag{66a}$$

$$O_{ij} = M_{ij} \tag{66b}$$

$$O_{ij} = f_{ij} \tag{66c}$$

with M_{ij} and f_{ij} being elements of the mass and force constant matrix, respectively. Eq. (66a) provides an estimate whether the two vectors **a** and **b** are spatially close, i.e. it measures their "spatial overlap". Eq. (66b) compares the two vectors kinetically ("mass comparison") and Eq. (66c) compares them dynamically ("force comparison"). Eqs. (66b) and (66c) reveal the influence of the atomic masses (*via* mass matrix **M**) or that of the electronic structure (*via* force constant matrix **f**) on the form of the normal mode l_μ.

The amplitude $A_{n\mu}$ defined in Eq. (64) can be considered as an "absolute amplitude". It is common practice to renormalize amplitudes and to express them as percentages according to Eq. (67):

$$A^{\%}_{n\mu} = \frac{A_{n\mu}}{\sum_m A_{m\mu}} 100 \tag{67}$$

to have a convenient way to compare them. This advantage has to be balanced against the fact that because of Eq. (67) amplitudes are no longer independent of the parameter set chosen.

According to which internal vibrational modes (**c**- or **a**-vectors: Cv or Av) and according to which metric **O** is used in Eq. (66) (**O** = **S**, **M**, **f**), different amplitudes can be defined, which are abbreviated in the following way:

$$\mathbf{O}=\mathrm{S}\begin{cases}\mathrm{AvAS} & \mathrm{AvPS}\\ \mathrm{CvAS} & \mathrm{CvPS}\end{cases} \tag{68}$$

$$\mathbf{O}=\mathrm{M}\begin{cases}\mathrm{AvAM} & \mathrm{AvPM}\\ \mathrm{CvAM} & \mathrm{CvPM}\end{cases} \tag{69}$$

$$\mathbf{O}=\mathrm{f}\begin{cases}\mathrm{AvAF} & \mathrm{AvPF}\\ \mathrm{CvAF} & \mathrm{CvPF}\end{cases} \tag{70}$$

where also the notation for **P** matrix based "amplitudes" used in the PED analysis [25-27] and discussed in Ref. 20 have been added.

On purely theoretical grounds as well as on application examples it has been shown [20,21] that only two of the twelve amplitudes given in Eqs. (68), (69), and (70), namely AvAF and AvAM, are suitable for the task of comparing ω_μ with ω_n or decomposing $\mathbf{l}_\mu$ in terms of $\mathbf{v}_n$. The six Cv... amplitudes based on **c**-vectors are largely unstable with regard to changes in the internal coordinates chosen to describe a molecule and, therefore, they are not suited for a comparison of normal modes and internal modes. On theoretical grounds, the A-type amplitudes are clearly superior to the P-type amplitudes of the PED analysis, [25-27] which excludes the six **P**-based amplitude definitions of Eqs. (68), (69), and (70). A spatial comparison of two vectors or functions, although a common practice when one considers dipole moments, orbitals, etc., provides little information in the case of the dynamic process of vibrating molecules. Therefore, it is more useful to use as metric matrix either the mass matrix **M** (kinematic comparison) or the force constant matrix **f** (dynamic comparison), which leaves of the twelve possible amplitudes just AvAM and AvAF as amplitudes suitable for a comparison of normal modes and internal modes within the CNM analysis.

A short summary of these results is provided in Figure 3, which shows frequency uncertainty tests in form of $A_{n\mu}$-$\Delta\omega_{\mu n}$ diagrams, in which normalized amplitudes $A_{n\mu}$ are plotted as a function of frequency differences $\Delta\omega_{\mu n}$ for the benzocyclobutadiene molecule. Amplitudes and frequencies were calculated at the HF/6-31G(d,p) level of theory for both a nonredundant set of internal coordinates (Figures 3a - 3d) and a strongly redundant set of internal coordinates (Figures 3e - 3h), which are described in Ref. 21. Amplitudes AvAF, AvPF, CvAF, and CvPF are employed in connection with adiabatic internal frequencies and **c**-vector frequencies.

In Figures 3a-3d, there are relatively large differences between the correlation patterns for Av- and Cv-type amplitudes where the former lead to clearly better results. In view of an expected Lorentzian-shaped correlation pattern $A_{n\mu}$-$\Delta\omega_{n\mu}$, the worst result is obtained in the case of the CvPF amplitudes of the PED analysis, which indicates that the PED approach is a rather poor basis for carrying out a CNM investigation. Replacing the P-type amplitude by the corresponding A-type amplitude as in the CvAF diagram improves the situation somewhat, however, there are still severe shortcomings of the description, which is obviously a result of the shortcomings of the **c**-vectors [19].

Clearly, the best correlation pattern complying exactly with the expected Lorentzian form is obtained in the case of the AvAF amplitudes in connection with a comparison of frequencies ω_μ with adiabatic internal frequencies ω_a. Adiabatic internal modes, the amplitude definition of Eq. (64) and the force constant matrix **f** as a suitable metric for comparison provide the right ingredients for a physically well-founded CNM analysis.

Using a redundant internal coordinate set as in the case of Figures 3e - 3h, a significant improvement of all correlation patterns can be observed. This has to do with the fact that with increasing size of the redundant parameter set **c**-vectors adopt more the form of **a**-vectors [19]. For example, in the case of the nonredundant internal coordinate set the average overlap between adiabatic and **c**-vectors is 0.69, which means that the two types of internal mode vectors are

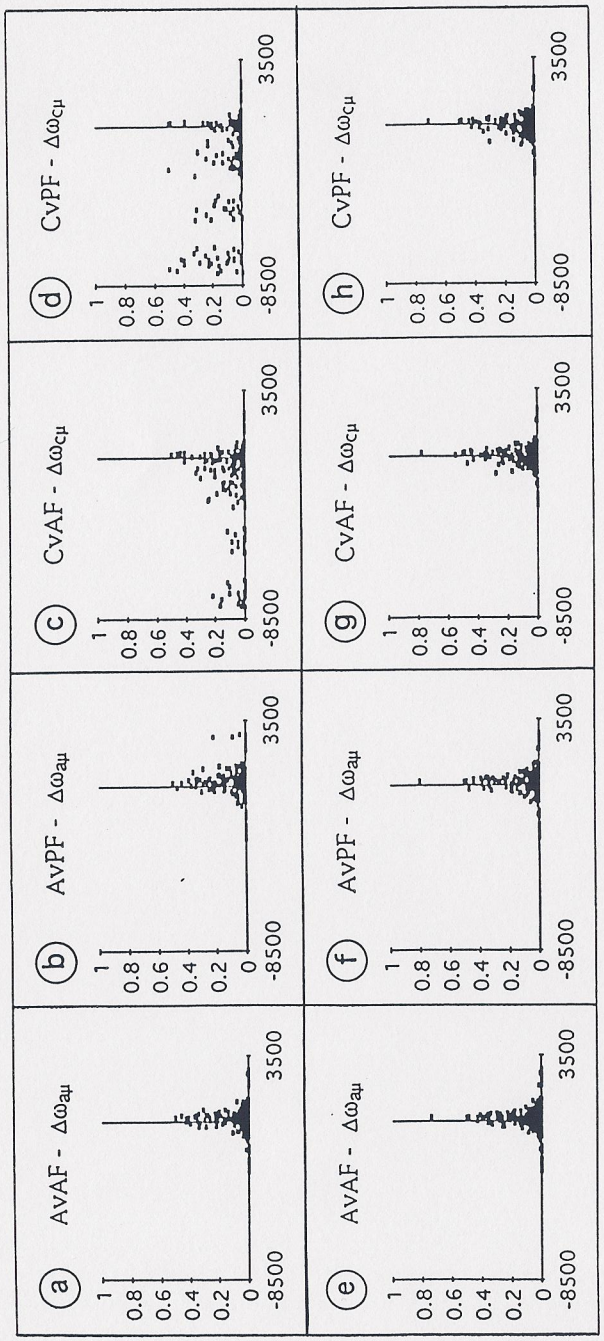

Figure 3. Frequency uncertainty test for benzocyclobutadiene according to HF/6-31G(d,p) calculations. The correlation diagrams correspond to correlations between normalized amplitudes $A_{n\mu}$ and frequency differences $\Delta\omega_{n\mu} = \omega_n - \omega_\mu$ with ω_n being a normal mode frequency of a molecular fragment ϕ_n and ω_μ being a normal mode frequency. Amplitudes AvAF, AvPF, CvAF, CvPF are employed in connection with adiabatic internal frequencies ω_a and c-vector frequencies ω_c using a nonredundant set of internal coordinates (a - d) or a strongly redundant set (e - h). In all cases, points that have $\Delta A = 0$ for all tests within a given row of diagrams are removed.

indeed significantly different. In the case of the redundant coordinate set, the average overlap has increased to 0.84 without changing the form of the **a**-vectors from that of the nonredundant coordinate set ($\mathbf{a}_n$ is completely independent of the set of internal coordinates chosen), i.e. with increasing number of internal coordinates, **c**-vectors will approach more and more the form of adiabatic vectors $\mathbf{a}_n$, which accordingly should be considered as the physically most reasonable internal vibrational mode vectors.

The 8 diagrams of Figure 3 clearly demonstrate the superiority of adiabatic internal mode vectors: They are independent of the choice of internal coordinates and determined just by the electronic structure of the molecule investigated. Obviously, one can improve in critical cases the usefulness of **c**-vectors by using larger and larger redundant parameter sets, however this solution cannot be generalized so that in general **a** vectors will always be superior to **c** vectors.

9. ANALYSIS OF VIBRATIONAL SPECTRA IN TERMS OF ADIABATIC INTERNAL MODES

A characterization of vibrational normal modes in terms of adiabatic internal modes is straightforward with the definitions given in the previous sections. As an example, the vibrational modes of cyclopropane [28] will be discussed. They have been calculated at the HF/6-31G(d,p) level of theory and they are compared with experimental frequencies in Table 1.

The normal modes of cyclopropane (see Figure 4) are easy to characterize because most of them involve motions associated with the same type of internal coordinate as, e.g., all six CH bond lengths (mode #1) or all three CH_2 twisting parameters (mode #5). Strong coupling between different types of internal parameters can only be found for modes #2, #10, #13 and #14 (Table 1). In the first two cases, CC stretching motions are mixed in, which becomes obvious from the pictorial representation of these modes given in Figure 4. However, these representations are sometimes misleading as can be seen from mode #3. According to the pictorial representation, one might expect that the ring breathing motion is connected with a CH scissoring or CH stretching motion, but the adiabatic analysis shows that mode #3 does not involve CH_2 scissoring or CH stretching. The arrows at the H atoms are simply a consequence of the movement of the C atoms. Modes #13 and #14 are a result of strong coupling between adiabatic CH_2 rocking and CH_2 twisting motions that is quantitatively described in the adiabatic mode analysis of Table 1.

Adiabatic frequencies of cyclopropane are compared in Table 2 with those of some other hydrocarbons [28]. The adiabatic CC frequency is about 40 and the adiabatic CH stretching frequency about 130 cm^{-1} larger than the corresponding values for cyclohexane. Compared to ethene, the adiabatic CH stretching frequencies are almost identical, which is in line with the high dissociation energy of the CH bond of cyclopropane [29]. The same observation has been made

Table 1
Analysis of the normal modes of cyclopropane using adiabatic internal modes. [a]

#	Sym	Frequencies exp.	HF, sc.	MP2, sc.	Characterization	Number of internal parameters
1	a_1'	3038	3130	3077	CH stretch (96%)	CH: (6 x 16%)
2		1479	1570	1496	CH_2 scissoring def (81%) + CC stretch (18%)	CH_2: (3 x 27%) + CC (3 x 6%)
3		1188	1238	1182	CC stretch (90%)	CC stretch: (3 x 30%)
4	a_2'	1070	1158	1043	CH_2 wag (99%)	CH_2 wag (3 x 33%)
5	a_1''	1126	1197	1129	CH_2 twist (99%)	CH_2 twist (3 x 33%)
6	a_2''	3102	3211	3184	CH stretch (100%)	CH stretch (6 x 16.7%)
7		854	873	846	CH_2 rock (99%)	CH_2 rock (3 x 33%)
8	e'	3024	3117	3067	CH stretch (100%)	CH stretch (4 x 25%)
					CH stretch (66%)	CH stretch (2 x 33%)
9		1438	1515	1439	CH_2 def (98%)	CH_2 def (66% + 17% + 16%)
					CH_2 def (98%)	CH_2 def (2 x 49%)
10		1028	1113	1043	CH_2 wag (86%) + CC stretch (9%)	CH_2 wag (48% + 38%)+CC (9%)
					CH_2 wag (86%) + CC stretch (14%)	CH_2 wag (57+ 9+20%) + CC stretch (8+6%)
11		868	911	872	CC stretch (88%)	CC stretch (64% + 24%)
					CC stretch (96%)	CC stretch (55% + 41%)
12	e"	3082	3189	3168	CH stretch (98%)	CH stretch (2 x 25% + 2 x 24%)
					CH stretch (66%)	CH stretch (2 x 33%)
13		1188	1271	1177	CH_2 rock (34%) + CH_2 twist (49%)	CH_2 rock (34%) + CH_2 twist (25+24%)
					CH_2 rock (51%) + CH_2 twist (33%)	CH_2 rock (26+25%) + CH_2 twist (33%)
14		739	744	734	CH_2 twist (56%) + CH_2 rock (30%)	CH_2 twist (2 x 28%) + CH_2 rock (30%)
					CH_2 rock (44%) + CH_2 twist (37%)	CH_2 rock (2 x 22%) + CH_2 twist (37%)

[a] All frequencies in cm^{-1}. Scaled HF/6-31G(d,p) and MP2/(9s5p1d/4s1p)[4s2p1d/2s1p] frequencies; scaling factors are 0.87 (HF) and 0.95 (MP2), respectively. Each normal mode is dissected into adiabatic internal vibrations [28]. The notation CH: (6 x 16%) implies that all six CH stretching modes (each with 16%) of cyclopropane contribute to the normal mode #1.

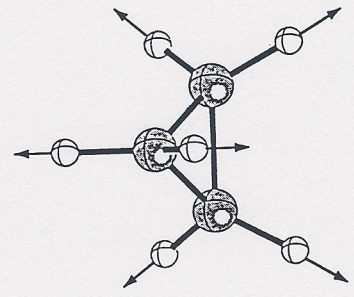

#1, a_1', in phase CH_2 sym. stretch

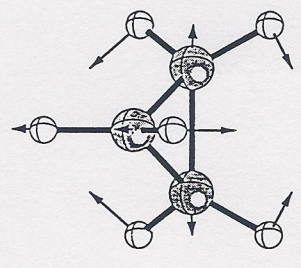

#2, a_1', CH_2 sym. scissor def

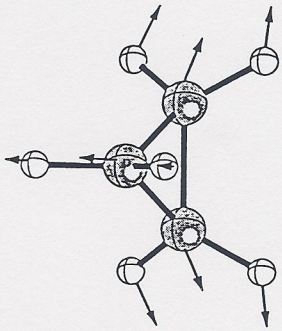

#3, a_1', C-C ring breath

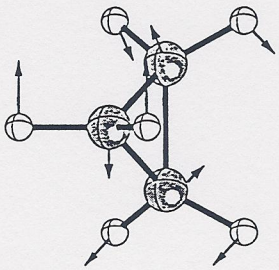

#4, a_2', CH_2 wag

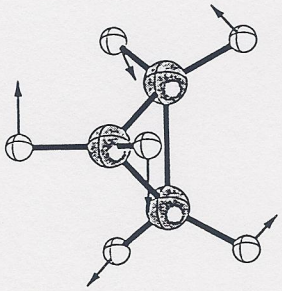

#5, a_1'', CH_2 twist

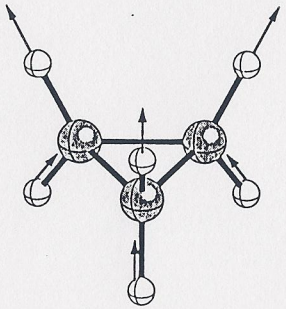

#6, a_2'', in phase CH_2 asym. stretch

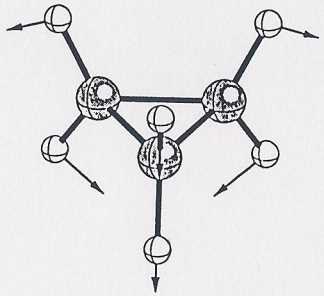

#7, a_2'', CH_2 rock

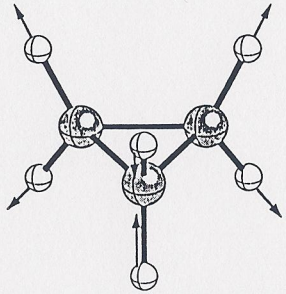

#8, e', out of phase CH_2 sym. stretch

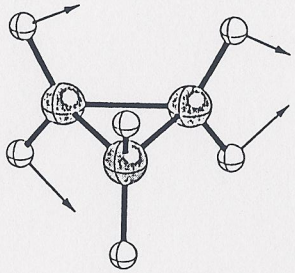

#9, e', CH_2 asym scissor def

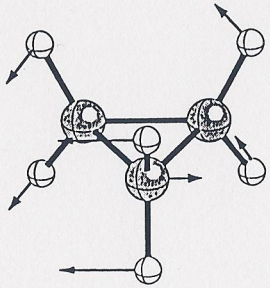

#10, e', CH_2 wag

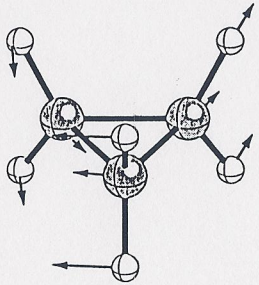

#11, e', C-C ring def

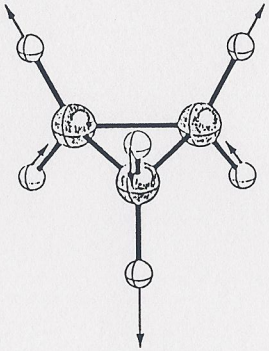

#12, e'', out of phase CH_2 asym. stretch

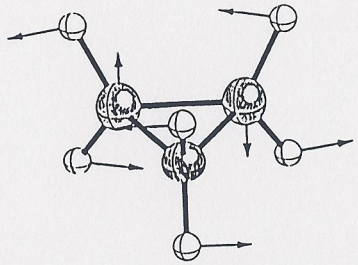

#13, e'', CH_2 rock + CH_2 twist

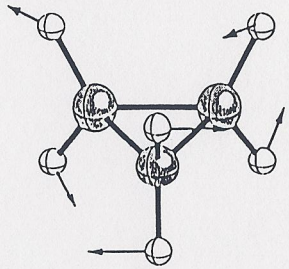

#14, e'', CH_2 twist + CH_2 rock

Figure 4. Vibrational modes of cyclopropane as obtained at the HF/6-31G(d,p) level of theory. Arrows indicate the direction and amplitude of each atomic motion. Symmetry assignments and a characterisation of each mode is also given in line with the notations used in Table 1.

by McKean using isolated CH frequencies obtained by appropriate deuteration of cyclopropane [30].

Table 2
Adiabatic internal frequencies of cyclopropane and some simple hydrocarbons. [a]

Molecule	CC stretch	CH stretch	HCH def
Ethene	1798	3344	1626
Cyclopropane	1169	3328	1614
Cyclobutane	1114	3222 (ax) 3233 (eq)	1621
Cyclohexane	1132	3172 (ax) 3200 (eq)	1621
Propane	1143	3192	1623

[a] All frequencies in cm^{-1}. HF/6-31G(d,p) calculations from Ref. 28.

As a second example, the CNM analyses of two related three-membered ring molecules, namely dioxirane (**1**) [31] and difluorodioxirane (**2**) [32], are given in Table 3. The analyses reveal how the vibrational modes change upon replacement of the two H atoms in **1** by two F atoms. Mode #1 of **2** is dominated by symmetric CO stretching (63%), however, it possesses also a strong admixture of symmetric CF stretching (30%) and 5% of CF_2 scissoring, which is contrary to **1** where just 9.5% OO stretching are mixed into this mode. Mode #2 is made up of 60% symmetric CF stretching, 27% OO stretching and 13% symmetric CO stretching. Again, this differs from the situation in **1** where mode #2 is a pure symmetric CH stretching mode. Clearly, these differences result from the fact that by a replacement of H atoms by F atoms mass coupling of the normal modes is increased.

Modes #3 (84% OO stretching), #4 (88% CF_2 scissoring), #5 (100% CF_2 twisting), and #7 (92 % CF_2 rocking) of **2** are less coupled with remaining contributions (see Table 3) being < 10%. Again, strong coupling is found in modes #6 (78% asymmetric CF stretching, 22% CF_2 rocking), #8 (67% asymmetric CO stretching, 33 % CF_2 wagging), and #9 (73% CF_2 wagging and 27% asymmetric CO stretching). In the case of **1**, just two of the nine normal modes, namely the two symmetrical ring stretching modes, modestly couple with each other (admixtures < 10%) while all other modes are almost uncoupled. This strikingly shows the influence of mass in mode coupling.

The calculated adiabatic frequencies reveal that the CO stretching modes increase by 70 cm^{-1} upon geminal F-substitution while the uncoupled OO stretching mode frequency decreases by just 44 cm^{-1}. Compared to oxirane (adiabatic CO stretching ω: 1130 cm^{-1}), the adiabatic CO stretching frequency of **1** (1121 cm^{-1}, Table 3) is normal while it is considerably increased for **2** (1189 cm^{-1}).

Table 3
Characterization of normal modes in terms of adiabatic internal modes for difluorodioxirane and dioxirane. [a]

#	Sym	exp.	Difluorodioxirane (2) CCSD(T),sc.	Difluorodioxirane (2) Characterization	Dioxirane (1) CCSD(T)	Dioxirane (1) Characterization	Adiabatic Frequencies 2	Adiabatic Frequencies 1
1	a_1	1467	1470	62.6% CO sym. str. (29.3% CF sym. str.; 5.5% CF_2 scissor)	1311	89.4% CO sym. str. (9.5% OO str.)	1189, CO	1121, CO
2	a_1	918	910	60.3% CF sym. str. (27.2% OO str.; 12.5% CO sym. str.)	3109	99.5% CH sym. str.	1200, CF	3180, CH
3	a_1	658	658	84% OO str. (8.9% CF sym. str.; 7% CO sym. str.)	759	93.4% OO str. (6.1% CO sym. str.)	800, OO	844, OO
4	a_1	511	512	88% CF_2 scissor 5.6% CO sym. str.	1578	93.8% CH_2 scissor	688, FCO	1267, HCO
5	a_2	416	389	100% CF_2 twist	1050	100% CH_2 twist	688, FCO	1267, HCO
6	b_1	1260	1259	78.2% CF asym. str. (21.8% CF_2 rock)	3187	99.9% CH asym. str.	1200, CF	3180, CH
7	b_1	557	559	92.5% CF_2 rock (7.5% CF asym. str.)	1200	99.9% CH_2 rock	688, FCO	1267, HCO
8	b_2	1062	1068	66.7% CO asym. str. (33.3% CF_2 wag)	931	99.6% CO asym. str.	1189, CO	1121, CO
9	b_2	621	617	73.2% CF_2 wag (26.8% CO asym. str.)	1292	96.1% CH_2 wag	688, FCO	1267, HCO

[a] Normal mode frequencies [cm^{-1}] for **1** from Ref. 31 (CCSD(T)/cc-VTZ2P+f,d), for **2** from Ref. 32 (CCSD(T)/cc-VTZ2P+f) and from Ref. 33 (exp.). Decomposition of normal modes in %. Second and third contributions are given in parentheses to facilitate reading. Adiabatic frequencies in cm^{-1} according to MP2(full)/cc-VTZ2P calculations are given with regard to internal coordinates specified after each frequency as CO for CO stretching frequency, FCO as FCO bending frequency, etc.

This indicates typical changes in the CO bond strength upon geminal F substitution in **1**.

As indicated for **1** and **2**, the CNM analysis in terms of adiabatic internal modes makes it rather simple to correlate the vibrational spectra of related molecules and to discuss the influence of substituents, heteroatoms, and structural changes in terms of the internal mode frequencies. In the following section, we will provide further examples how vibrational spectra of different molecules can be correlated with the help of the CNM analysis.

10. CORRELATION OF VIBRATIONAL SPECTRA OF DIFFERENT MOLECULES

The CNM analysis in terms of adiabatic internal modes has been carried out to correlate the calculated vibrational spectra of the three dehydrobenzenes, namely *ortho*- (**3**), *meta*- (**4**) and *para*-benzyne (**5**), with the vibrational spectrum of benzene (**6**). Investigation of dehydrobenzenes with the help of infrared spectroscopy is of considerable interest at the moment since these molecules have been found to represent important intermediates in the reaction of enediyne anticancer drugs with DNA molecules [34-37]. Both **4** and **5** are singlet biradicals and, therefore, they are so labile that they can only be trapped at low temperatures in an argon matrix upon photolytic decomposition of a suitable precursor [38-40].

A positive identification of the dehydrobenzenes in the matrix requires, besides an expert set up of the experiment, high level *ab initio* calculations of the infrared spectra of the compounds trapped so that comparison between measured and calculated spectra becomes meaningful. In this way, both **4** and **5** have been identified and investigated in the matrix [38,39]. To further understand the electronic nature and the relationship of the three dehydrobenzenes, a correlation of their calculated vibrational spectra is desirable.

Kraka and co-workers [41] have calculated the vibrational spectra of **3**, **4**, and **5** at the GVB(1)/6-31G(d,p) level of theory where in each case the biradical nature of the dehydrobenzenes was described by the two-configuration approach of GVB. In Tables 4, 5, and 6, a CNM analysis of the calculated spectra based on calculated adiabatic internal modes is presented.

With the CNM analyses presented in Tables 4, 5, and 6 and a similar analysis for benzene, it is straightforward to correlate the vibrational spectra of the three benzynes with each other and with that of benzene. This is done in Tables 7, 8, and 9, which should be read considering that benzene has 30 normal modes while the benzynes have only 24. Hence, not all normal modes of benzene can be correlated with normal modes of the benzynes.

Tables 7, 8, and 9 are the basis for the correlation diagram shown in Figure 5 that compares the calculated infrared spectra of the three benzynes with that of benzene. Only the normal modes with infrared intensities larger than 0.1 are considered in this comparison. The numbers in parentheses denote the mode numbers used in Tables 4-9. Dashed lines connect infrared bands that are related according to the CNM analyses presented in Tables 4, 5, and 6.

Table 4
CNM analysis of the vibrational spectrum of 1,2-didehydrobenzene (*o*-benzyne, **3**) calculated at the GVB(1)/6-31G(d,p) level of theory. [a]

#	Sym	Freq	Characterization	Detailed characterization
24	a_1	3387	HC(88%)	HC(2*44)
23	b_2	3384	HC(94%)	HC(2*47)
22	a_1	3358	HC(86%)	HC(2*43)
21	b_2	3341	HC(94%)	HC(2*47)
20	a_1	1942	CC(66%)	CC(66%)
19	b_2	1688	CC(40%)+HCC(30%)	CC(2*20)+HCC(2*8+2*7)
18	a_1	1607	HCC(58%)+CC(30%)	HCC(2*15+2*14)+CC(20+10)
17	b_2	1559	HCC(62%)+CC(30%)	HCC(2*24+2*7)+CC(2*15)
16	a_1	1398	HCC(46%)+CC(37%)	HCC(2*16+2*7)+CC(2*15+7)
15	b_2	1362	HCC(58%)+CC(34%)	HCC(2*29)+CC(2*17)
14	a_1	1234	CC(53%)+HCC(44%)	CC(17+2*14+8)+HCC(2*22)
13	b_2	1210	HCC(50%)+CC(38%)	HCC(2*16+2*11)+CC(2*19)
12	a_2	1106	HCCC(78%)+CCCC(19%)	HCCC(2*28+2*11)+CCCC(19)
11	a_1	1104	CC(68%)+HCC(8%)	CC(2*34)+HCC(2*4)
10	a_1	1086	CC(76%)+HCC(10%)	CC(44+2*16)+HCC(2*5)
9	b_1	1057	HCCC(90%)	HCCC(2*28+2*17)
8	a_2	974	HCCC(96%)	HCCC(2*33+2*15)
7	b_2	969	CCC(98%)	CCC(2*28+2*14+2*7)
6	b_1	833	HCCC(98%)	HCCC(2*25+2*24)
5	a_2	692	CCCC(91%)	CCCC(20+2*17+2*13+11)
4	a_1	657	CCC(68%)	CCC(2*34)
3	b_2	593	CCC(92%)	CCC(2*36+2*10)
2	a_2	493	CCCC(91%)	CCCC(37+20+2*17)
1	b_1	448	CCCC(90%)	CCCC(2*26+2*19)

[a] Frequencies in cm^{-1}. The following notation is used: CC: CC stretching; HC: HC stretching; CCC: CCC bending; HCC: HCC bending; CCCC: ring torsion; HCCC(op): hydrogen out-of-plane bending. The last column gives a detailed analysis of each normal mode in terms of adiabatic modes. E.g., normal mode #18 is described by 58% HCC in-plane bending and 30% CC stretching. The HCC in-plane bending comprises four different HCC bending modes, two with 15% and two with 14%, and the CC stretching mode comprises two different CC stretching modes, one with 20% and one with 10%.

Table 5
CNM analysis of the vibrational spectrum of 1,3-didehydrobenzene (*m*-benzyne, **4**) calculated at the GVB(1)/6-31G(d,p) level of theory. [a]

#	Sym	Freq	Characterization	Detailed characterization
24	a_1	3420	HC(99%)	HC(99%)
23	a_1	3377	HC(99%)	HC(42+41+16)
22	b_2	3371	HC(100%)	HC(2*50)
21	a_1	3342	HC(82%)	HC(82%)
20	a_1	1792	CC(68%)	CC(2*24+2*10)
19	b_2	1685	CC(42%)+HCC(26%)	CC(2*21)+HCC(26)
18	a_1	1552	HCC(49%)+CC(42%)	HCC(25+24)+CC(2*12+2*10)
17	b_2	1544	HCC(64%)	HCC(20+17+16+11)
16	a_1	1384	HCC(89%)	HCC(61+2*14)
15	b_2	1313	CC(60%)+HCC(27%)	CC(2*16+2*14)+HCC(27)
14	b_2	1201	CC(64%)+HCC(31%)	CC(2*17+2*15)+HCC(2*9+8+5)
13	a_1	1183	HCC(46%)+CC(26%)	HCC(2*23)+CC(2*13)
12	a_1	1109	CC(68%)	CC(2*18+2*16)
11	b_1	1102	HCCC(83%)	HCCC(57+2*13)
10	b_2	1068	CC(70%)	CC(2*24+2*11)
9	a_1	977	CCC(90%)	CCC(2*24+22+2*10)
8	a_2	966	HCCC(92%)	HCCC(2*46)
7	b_1	953	HCCC(80%)	HCCC(76+4)
6	b_1	857	HCCC(71%)	HCCC(23+2*18+12)
5	b_1	685	CCCC(94%)	CCCC(4*16+2*15)
4	b_2	655	CCC(96%)	CCC(2*26+2*22)
3	a_2	532	CCCC(60%)	CCCC(2*30)
2	a_1	531	CCC(96%)	CCC(39+21+2*18)
1	b_1	447	CCCC(82%)	CCCC(2*22+2*19)

[a] See footnote in Table 4.

Table 6
CNM analysis of the vibrational spectrum of 1,4-didehydrobenzene (*p*-benzyne, **5**) calculated at the GVB(1)/6-31G(d,p) level of theory. [a]

#	Sym	Freq	Characterization	Detailed characterization
24	a_g	3379	HC(100%)	HC(4*25%)
23	b_{2u}	3378	HC(100%)	HC(4*25%)
22	b_{3g}	3362	HC(100%)	HC(4*25%)
21	b_{1u}	3361	HC(100%)	HC(4*25%)
20	b_{3g}	1785	CC(72%)	CC(4*18%)
19	a_g	1646	CC(36%)+HCC(24%)	CC(2*18%)+HCC(4*6%)
18	b_{1u}	1604	HCC(64%)	HCC(4*16%)
17	b_{2u}	1456	HCC(40%)+CC(22%)	HCC(4*10%)+CC(2*11%)
16	b_{3g}	1397	HCC(92%)	HCC(4*23%)
15	b_{2u}	1297	CC(64%)+HCC(28%)	CC(4*16%)+HCC(4*7%)
14	a_g	1250	HCC(76%)	HCC(4*19%)
13	b_{1u}	1124	CC(52%)+HCC(28%)	CC(4*13%)+HCC(4*7%)
12	b_{2u}	1117	CC(64%)+HCC(16%)	CC(2*32%)+HCC(4*4%)
11	a_g	1097	CC(98%)	CC(2*17%+4*16%)
10	a_u	1080	HCCC op(88%)	HCCC op(4*22%)
9	b_{1u}	1050	CCC(100%)	CCC(2*20%+4*15%)
8	b_{2g}	1042	HCCC op(76%)	HCCC op(4*19%)
7	b_{1g}	897	HCCC op(100%)	HCCC op(4*25%)
6	b_{3u}	853	HCCC op(88%)	HCCC op(4*22%)
5	b_{2g}	715	CCCC(96%)	CCCC(6*16%)
4	a_g	662	CCC(60%)	CCC(2*30%)
3	b_{3g}	640	CCC(96%)	CCC(4*24%)
2	b_{3u}	492	CCCC(100%)	CCCC(4*25%)
1	a_u	464	CCCC(62%)	CCCC(2*31%)

[a] See footnote in Table 4.

Table 7
Correlation of the normal modes of benzene (6) with those of 1,2-didehydrobenzene (*o*-benzyne, 3). [a]

	Benzene		*ortho*-Benzyne		
#	Sym	Characterization	#	Sym	Characterization
30	a_{1g}	sym HC st	24	a_1	HC(88%)
29	e_{1u}	asym HC st	23	b_2	HC(94%)
28	e_{1u}		-	-	-
27	e_{2g}	asym HC st	-	-	-
26	e_{2g}		22	a_1	HC(86%)
25	b_{1u}	asym HC st	21	b_2	HC(94%)
24	e_{2g}	ring st	20	a_1	CC(66%)
23	e_{2g}		19	b_2	CC(40%)+HCC(30%)
22	e_{1u}	ring def	-	-	-
21	e_{1u}		-	-	-
20	a_{2g}	HCC def	17	b_2	HCC(62%)+CC(30%)
19	b_{2u}	HCC def	16	a_1	HCC(46%)+CC(37%)
18	e_{2g}	HCC def	14	a_1	CC(53%)+HCC(44%)
17	e_{2g}		13	b_2	HCC(50%)+CC(38%)
16	b_{2u}	ring st	-	-	-
15	e_{1u}	HCC def	11	a_1	CC(68%)+HCC(8%)
14	e_{1u}		-	-	-
13	b_{2g}	H twist	12	a_2	HCCC(78%)+CCCC(19%)
12	e_{2u}	H twist	-	-	-
11	e_{2u}		9	b_1	HCCC(90%)
10	b_{1u}	asym ring breath	7	b_2	CCC(98%)
9	a_{1g}	sym ring breath	10	a_1	CC(76%)+HCC(10%)
8	e_{1g}	HC wagging	-	-	-
7	e_{1g}		8	a_2	HCCC(96%)
6	b_{2g}	chair o.p	5	a_2	CCCC(91%)
5	a_{2u}	HC wagging	6	b_1	HCCC(98%)
4	e_{2g}	ring def	3	b_2	CCC(92%)
3	e_{2g}		4	a_1	CCC(68%)
2	e_{2u}	twist boat o.p	2	a_2	CCCC(91%)
1	e_{2u}	boat o.p	1	b_1	CCCC(90%)

[a] For an explanation of the notation used, see Table 4.

Table 8
Correlation of the normal modes of benzene (6) with those of 1,3-didehydrobenzene (*m*-benzyne, 4). [a]

	Benzene		*meta*-Benzyne		
#	Sym	Characterization	#	Sym	Characterization
30	a_{1g}	sym HC st	23	a_1	HC(99%)
29	e_{1u}	asym HC st	23	a_1	HC(99%)
28	e_{1u}		22	b_2	HC(100%)
27	e_{2g}	asym HC st	22	b_2	HC(100%)
26	e_{2g}		21	a_1	HC(82%)
25	b_{1u}	asym HC st	21	a_1	HC(82%)
24	e_{2g}	ring st	20	a_1	CC(68%)
23	e_{2g}		19	b_2	CC(42%)+HCC(26%)
22	e_{1u}	ring def	18	a_1	HCC(49%)+CC(42%)
21	e_{1u}		17	b_2	HCC(64%)
20	a_{2g}	HCC def	16	a_1	HCC(89%)
19	b_{2u}	HCC def	15	b_2	CC(60%)+HCC(27%)
18	e_{2g}	HCC def	13	a_1	HCC(46%)+CC(26%)
17	e_{2g}		14	b_2	CC(64%)+HCC(31%)
16	b_{2u}	ring st	10	b_2	CC(70%)
15	e_{1u}	HCC def	13	a_1	HCC(46%)+CC(26%)
14	e_{1u}		-	-	-
13	b_{2g}	H twist	11	b_1	HCCC(83%)
12	e_{2u}	H twist	8	a_2	HCCC(92%)
11	e_{2u}		11	b_1	HCCC(83%)
10	b_{1u}	asym ring breath	9	a_1	CCC(90%)
9	a_{1g}	sym ring breath	12	a_1	CC(68%)
8	e_{1g}	HC wagging	8	a_2	HCCC(92%)
7	e_{1g}		7	b_1	HCCC(80%)
6	b_{2g}	chair o.p	5	b_1	CCCC(94%)
5	a_{2u}	HC wagging	6	b_1	HCCC(71%)
4	e_{2g}	ring def	2	a_1	CCC(96%)
3	e_{2g}		-	-	-
2	e_{2u}	twist boat o.p	3	a_2	CCCC(60%)
1	e_{2u}	boat o.p	1	b_1	CCCC(82%)

[a] For an explanation of the notation used, see Table 4.

Table 9
Correlation of the normal modes of benzene (**6**) with those of 1,4-didehydrobenzene (*p*-benzyne, **5**). [a]

	Benzene		*para*-Benzyne		
#	Sym	Characterization	#	Sym	Characterization
30	a_{1g}	sym HC st	24	a_g	HC(100%)
29	e_{1u}	asym HC st	21	b_{1u}	HC(100%)
28	e_{1u}		23	b_{2u}	HC(100%)
27	e_{2g}	asym HC st	22	b_{3g}	HC(100%)
26	e_{2g}		24	a_g	HC(100%)
25	b_{1u}	asym HC st	21	b_{1u}	HC(100%)
24	e_{2g}	ring st	19	a_g	CC(36%)+HCC(24%)
23	e_{2g}		20	b_{3g}	CC(72%)
22	e_{1u}	ring def	18	b_{1u}	HCC(64%)
21	e_{1u}		17	b_{2u}	HCC(40%)+CC(22%)
20	a_{2g}	HCC def	16	b_{3g}	HCC(92%)
19	b_{2u}	HCC def	15	b_{2u}	CC(64%)+HCC(28%)
18	e_{2g}	HCC def	14	a_g	HCC(76%)
17	e_{2g}		16	b_{3g}	HCC(92%)
16	b_{2u}	ring st	12	b_{2u}	CC(64%)+HCC(16%)
15	e_{1u}	HCC def	13	b_{1u}	CC(52%)+HCC(28%)
14	e_{1u}		13	b_{1u}	CC(52%)+HCC(28%)
13	b_{2g}	H twist	8	b_{2g}	HCCC op(76%)
12	e_{2u}	H twist	10	a_u	HCCC op(88%)
11	e_{2u}		6	b_{3u}	HCCC op(88%)
10	b_{1u}	asym ring breath	9	b_{1u}	CCC(100%)
9	a_{1g}	sym ring breath	11	a_g	CC(98%)
8	e_{1g}	HC wagging	7	b_{1g}	HCCC op(100%)
7	e_{1g}		-	-	-
6	b_{2g}	chair o.p	5	b_{2g}	CCCC(96%)
5	a_{2u}	HC wagging	6	b_{3u}	HCCC op(88%)
4	e_{2g}	ring def	4	a_g	CCC(60%)
3	e_{2g}		3	b_{3g}	CCC(96%)
2	e_{2u}	twist boat o.p	1	a_u	CCCC(62%)
1	e_{2u}	boat o.p	2	b_{3u}	CCCC(100%)

[a] For an explanation of the notation used, see Table 4.

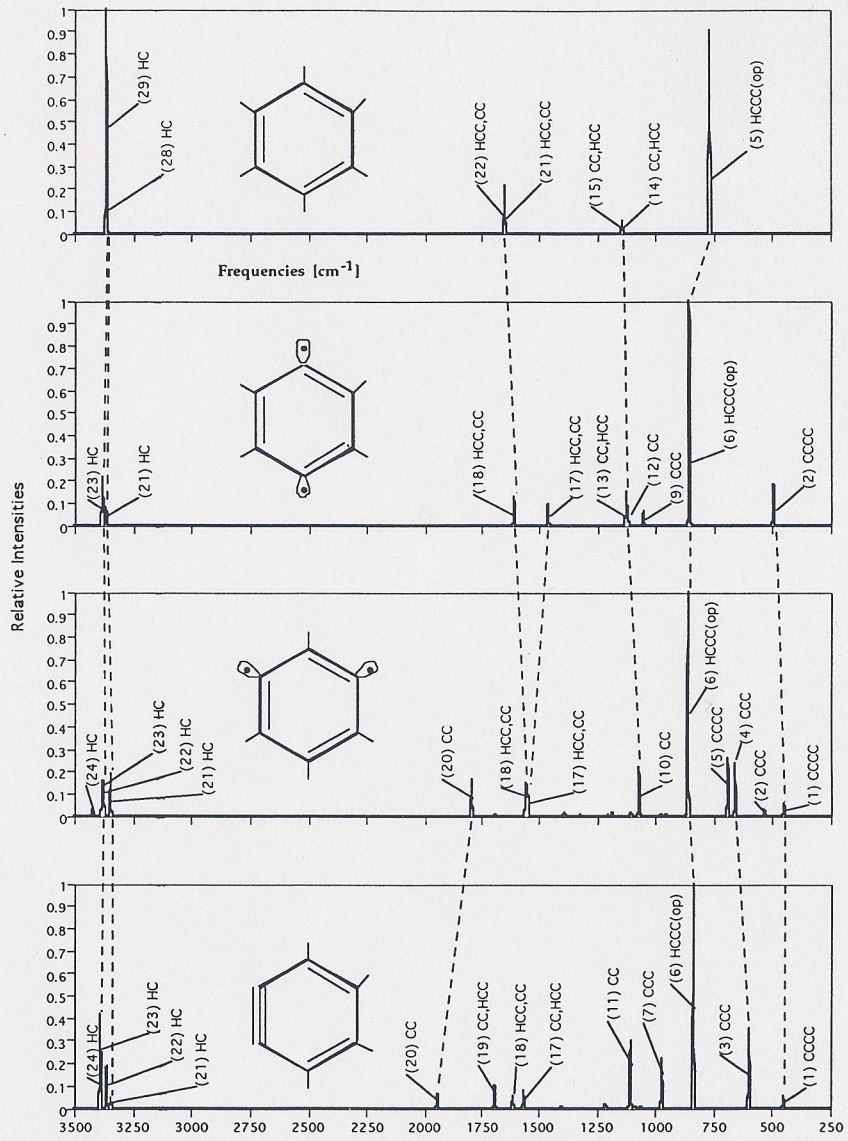

Figure 5. Correlation of the calculated infrared spectra of benzene (**6**), *para*-benzyne (**5**), *meta*-benzyne (**4**), and *ortho*-benzyne (**3**). For each infrared band, the corresponding mode number (in parentheses) and an appropriate characterization according to the CNM analysis of Tables 4 - 6 is given. Dashed lines correlate the infrared bands of different molecules.

Table 10
Adiabatic internal frequencies (in cm^{-1}) of *ortho*- (3), *meta*- (4) and *para*-benzyne (5) calculated at the GVB(1)/6-31(d,p) level of theory.

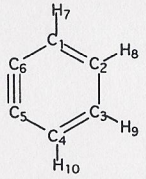

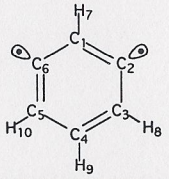

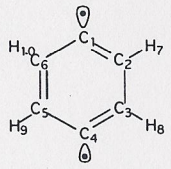

ortho-benzyne		*meta*-benzyne		*para*-benzyne	
Parameter	Freq	Parameter	Freq	Parameter	Freq
C5C6	1787	C1C2	1356	C1C2	1415
C2C3	1213	C1C6	1356	C1C6	1415
C1C6	1386	C2C3	1419	C3C4	1415
C4C5	1386	C5C6	1419	C4C5	1415
C1C2	1391	C3C4	1395	C2C3	1317
C3C4	1391	C4C5	1395	C5C6	1317
H7C1	3378	H7C1	3414	H7C2	3366
H10C4	3378	H9C4	3343	H8C3	3366
H8C2	3348	H8C3	3367	H9C5	3366
H9C3	3348	H10C5	3367	H10C6	3366
C1C6C5	739	C2C1C6	735	C1C2C3	953.8
C4C5C6	739	C3C4C5	963	C2C3C4	953.8
C2C1C6	919	C1C2C3	786	C4C5C6	953.8
C3C4C5	919	C1C6C5	786	C1C6C6	953.8
C1C2C3	1023	C2C3C4	963	C2C1C6	954.1
C2C3C4	1023	C4C5C6	963	C3C4C5	954.1
H7CC ip	1423	H7CC ip	1391	H7CC ip	1394
H10CC ip	1423	H9CC ip	1429	H8CC ip	1394
H8CC ip	1434	H8CC ip	1403	H9CC ip	1394
H9CC ip	1434	H10CC ip	1403	H10CC ip	1394
C1C6C5C4	560	C3C2C1C6	618	C3C2C1C6	638
C1C2C3C4	684	C2C1C6C5	618	C2C3C4C5	638
C2C1C6C5	581	C1C2C3C4	644	C3C4C5C6	638
C3C4C5C6	581	C1C6C5C4	644	C2C1C6C5	638
C3C2C1C6	646	C2C3C4C5	633	C1C2C3C4	639
C2C3C4C5	646	C3C4C5C6	633	C1C6C5C4	639
H7CCC op	957	H7CCC op	910	H7CCC op	945
H10CCC op	957	H9CCC op	1004	H8CCC op	945
H8CCC op	956	H8CCC op	920	H9CCC op	945
H9CCC op	956	H10CCC op	920	H10CCC op	945

The adiabatic internal frequencies calculated for the three benzynes are listed in Table 10 together with the associated internal coordinates. They have to be compared with the corresponding adiabatic frequencies of benzene obtained at the HF/6-31G(d,p) level of theory: CC 1406, HC 3348, CCC 997, HCC in-plane 1441, CCCC 653, and HCCC out-of-plane 969 cm^{-1}.

With the help of Figure 5, it is possible to identify the three benzynes and to discuss their electronic features. For example, **3** is best identified by its CC triple bond stretching frequency close to 1942 cm^{-1} (after scaling at 1690 cm^{-1}), which has a low intensity, but nevertheless should be observable since no other infrared bands appear in this region. Similarly, the boat-type ring torsion mode of **5** possesses contrary to the other molecules a stronger intensity in a region where no other infrared bands should appear (see Figure 5). In the case of **4**, it is the pattern of ring distortion modes in the region between 500 and 1500 cm^{-1} that facilitates its identification [38,39,41].

Similar correlations of vibrational spectra have been carried out with the help of the CNM analysis and the adiabatic frequencies for a number of molecules [40,41]. They all confirm the value of the CNM analysis that extends beyond a simple comparison of geometries. For example, in the case of the benzynes (Table 10), the adiabatic CC stretching frequencies do not correlate with the calculated CC equilibrium bond lengths. This has to do with the fact that, unlike to the equilibrium bond lengths, the adiabatic stretching frequencies are sensitive to the environment of the CC bonds. In **4**, bond C1C2 has a lower adiabatic frequency than bond C3C4 since a C1C2 stretching vibration leads to an increase of CH bond eclipsing strain and, therefore, this bond is stiffer. Bond C2C3, which one might expect to be comparable with bond C1C2, possesses an even higher adiabatic stretching frequency indicating in this way CC bond strengthening by through-bond interactions between the radical center C2 and the σ^*-orbital of bond C3C4 [36,37]. In a similar way, the other CC stretching frequencies listed in Table 10 can be discussed.

11. DERIVATION OF BOND INFORMATION FROM VIBRATIONAL SPECTRA

A serious attempt of associating measured normal mode frequencies with characteristic fragment frequencies was undertaken by McKean who investigated the stretching mode of the CH group in various hydrocarbons [30]. This author solved the problem of mode-mode coupling within the molecules investigated by D-substitution of all H atoms but the one considered thus increasing mass differences and reducing the amount of intramolecular mode-mode coupling. His approach led to characteristic CH stretching frequencies in different molecules and, by this, to an unique insight into the nature of the CH bond under different situations [30]. McKean could set up a linear relationship between the isolated CH stretching frequencies he measured and experimentally known CH bond lengths where both r_0 and r_s values had to be used. McKean suggested to employ this relationship for the determination of unknown CH bond lengths by infrared spectroscopy using measured CH stretching frequencies where he

predicted that this could be done with an accuracy of ±0.0005 Å which is better than the accuracy achieved when determining CH bond lengths by microwave spectroscopy. In Figure 6, the linear relationship between measured C-H stretching frequencies taken from the work of McKean and equilibrium C-H bond lengths calculated by Larsson and Cremer [42] is shown. Calculated rather than measured C-H bond lengths are used since they provide a more consistent description of the relationship between frequencies and bond lengths than the r_0 and r_s values used by McKean.

Certainly, it is possible to obtain other characteristic fragment frequencies in a systematic way although an enormous amount of synthetic work is involved to get suitable isotopomers in each case. In addition, the measured fragment frequencies will always be contaminated by some residual coupling. Therefore, one can predict that it is hardly possible to solve, just by experimental means, the problem of determining fragment-specific frequencies.

In this situation, an attractive alternative is provided by the adiabatic internal frequencies. For example, the McKean relationship between C-H stretching frequencies and equilibrium C-H bond lengths can easily be reproduced with the help of adiabatic CH stretching frequencies calculated at the HF/6-31G(d,p) level of theory as is shown in Figure 7. The r^2 coefficient obtained is 0.998, which is clearly better than the r^2 coefficient for the correlation of the experimental frequencies (0.991, Figure 6). Eq. (71) gives the relationship between C-H equilibrium bond lengths and internal frequencies, which can be used

$$r_e(C-H) = -8.0155\times10^{-5}\,\omega_e(C-H) + 1.3442 \qquad (71)$$

to calculate CH bond lengths once experimental values of isolated CH stretching frequencies are known. From a computational point of view, Eq. (72) is more useful since it provides C-H vibrational frequencies

$$\omega_e(C-H) = 16770 - 12476\; r_e(C-H) \qquad (72)$$

once the geometry of the molecule has been calculated.

Figure 7 confirms the McKean relationship [30] and, furthermore, suggests that calculated adiabatic internal frequencies are as useful or even more useful as the measured "isolated" C-H stretching frequencies. However, the real advantage of adiabatic frequencies will become obvious if one attempts to set up McKean relationships also for other bonds.

This question has been checked in the case of the CC bond [42]. In a molecule with more than one CC bond, individual CC stretching motions spread over several normal modes and there is mostly considerable coupling between the individual modes. To obtain "isolated" CC stretching frequencies similar as in the case of the CH bonds is impossible both for experimental and mass reasons. Synthesizing isotopomers, for which the C atoms of neighboring CC bonds are replaced by heavier isotopes just to "isolate" the CC bond under investigation would be a synthetically difficult and at the same time fruitless enterprise since a replacement of ^{12}C by ^{13}C or even ^{14}C isotopes means a too small change in the relative masses to achieve any effective mass decoupling. If one takes on the

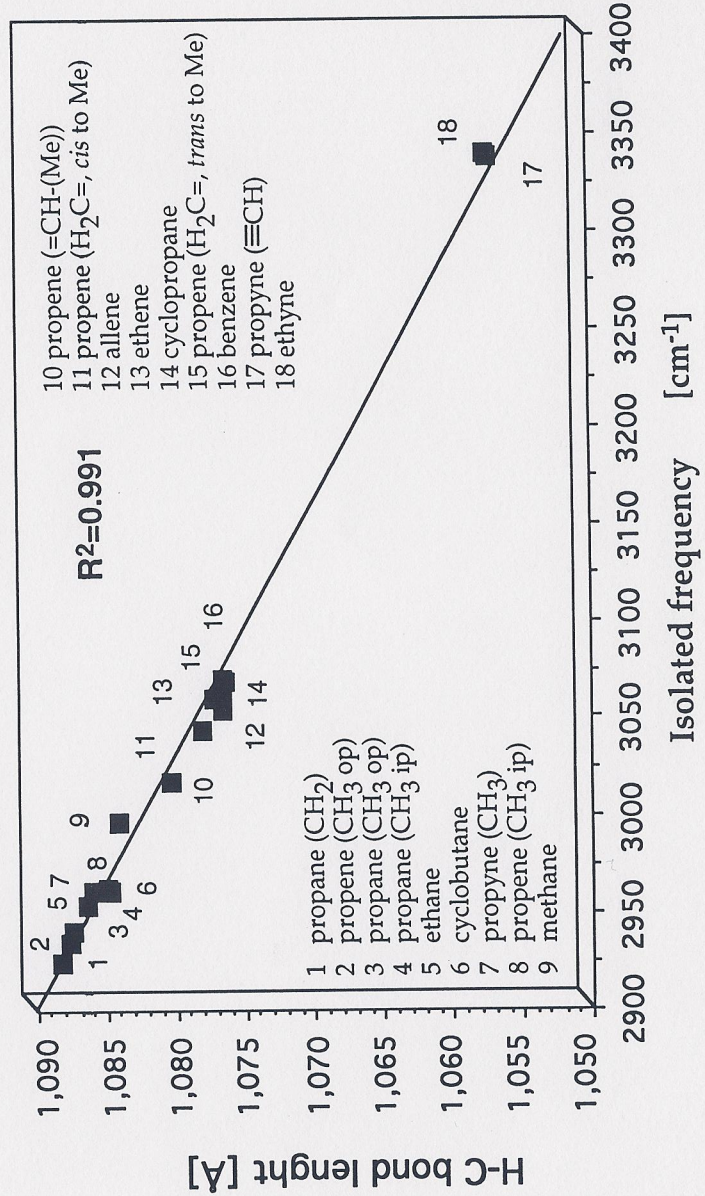

Figure 6. Linear correlation between CH bond lengths calculated at the HF/6-31G(d,p) level of theory [42] and the measured "isolated infrared frequencies" of McKean [30].

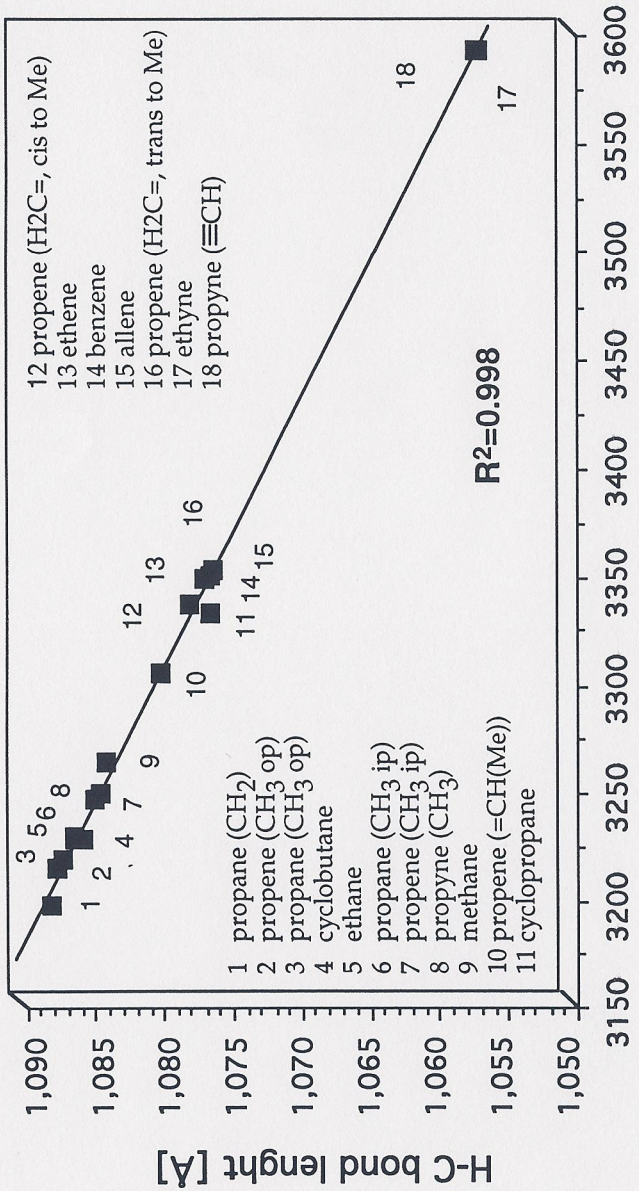

Figure 7. Linear correlation between CH bond lengths calculated at the HF/6-31G(d,p) level of theory and adiabatic CH stretching frequencies [42].

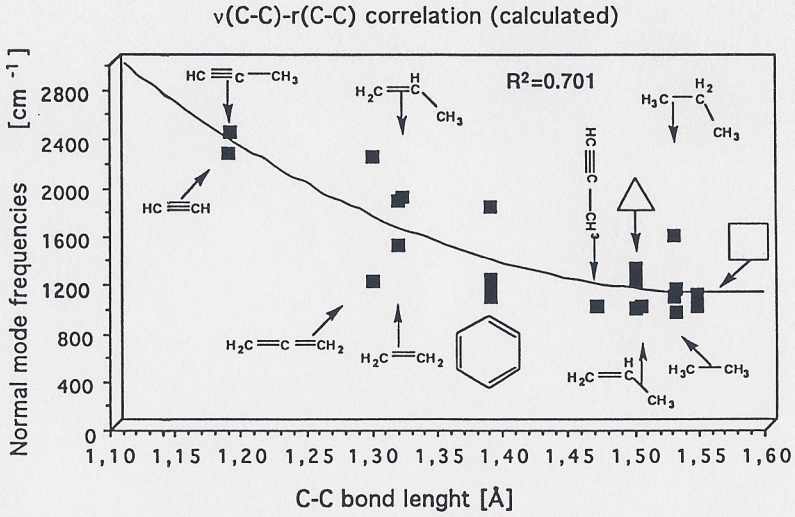

Figure 8. Quadratic correlation between normal mode frequencies generally considered to represent CC stretching frequencies and CC equilibrium bond lengths both calculated at the HF/6-31G(d,p) level of theory [42].

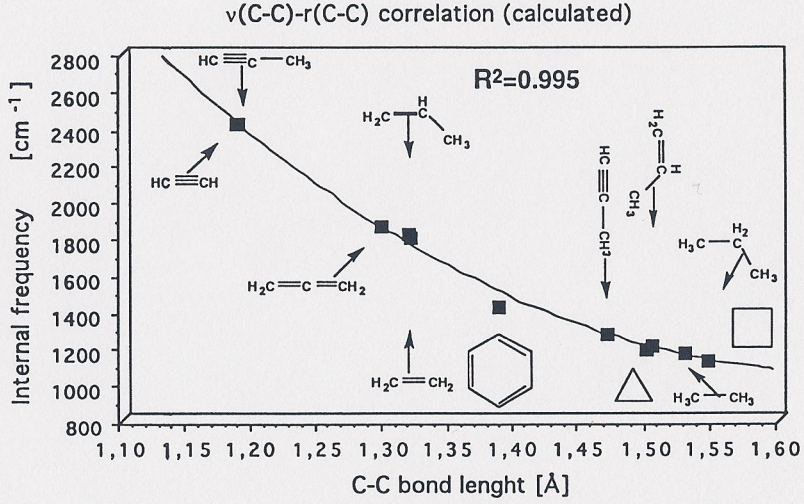

Figure 9. Quadratic correlation between adiabatic CC stretching frequencies and CC equilibrium bond lengths both calculated at the HF/6-31G(d,p) level of theory [42].

other hand the CC stretching modes in the way they are calculated in the normal mode analysis, then there is little correlation between CC stretching frequencies and equilibrium CC bond lengths as can be seen from Figure 8. There is a considerable scattering of CC stretching frequencies ($r^2 = 0.701$) around a ω_e/r_e relationship, which has basically quadratic form.

The problem can be solved by using adiabatic CC stretching frequencies derived from the normal mode frequencies of Figure 8 [42]. In Figure 9, a correlation between adiabatic CC stretching frequencies and CC equilibrium bond lengths is shown, which is best represented by the quadratic Eq. (73):

$$\omega_e(CC) = 18196 - 20742\ r_e(CC) + 6268\ [r_e(CC)]^2 \qquad (73)$$

which leads to a correlation coefficient $r^2 = 0.995$.

One can use stretching frequency/bond length relationships to predict geometrical features of molecules from measured infrared spectra. This should be first checked for a case where verification of the prediction is possible due to an available geometry obtained from an *ab initio* calculation.

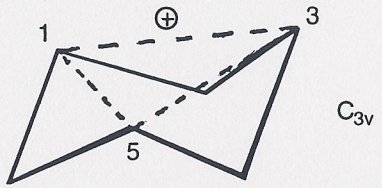

The trishomotropenylium cation contains a homoaromatic 2-electron-3-center system with long 1,3 distances [43]. If one calculates the adiabatic C1C3 stretching mode for this system at the MP2/6-31G(d,p) level of theory, one gets a value of 556 cm^{-1}. Using the quadratic relationship between stretching frequencies and CC distances shown in Figure 10, one obtains a C1C3 distance of 1.82 Å, which is almost identical with the calculated MP2/6-31G(d,p) distance [43]. Hence, the example shows that distances can be reliably predicted once the value of the internal frequency is known.

12. ADIABATIC INTERNAL MODES FROM EXPERIMENTAL FREQUENCIES

Ab initio frequencies of normal vibrational modes and, by this also, adiabatic frequencies suffer from the harmonic approximation used in the calculation. Even when applying efficient scaling procedures, there is no guarantee that *ab initio* frequencies accurately reproduce the exact fundamental frequencies of the experiment. Therefore, one has to ask whether the adiabatic internal frequencies might not be much more meaningful if they would be based on experimental frequencies rather than frequencies calculated within the harmonic approximation.

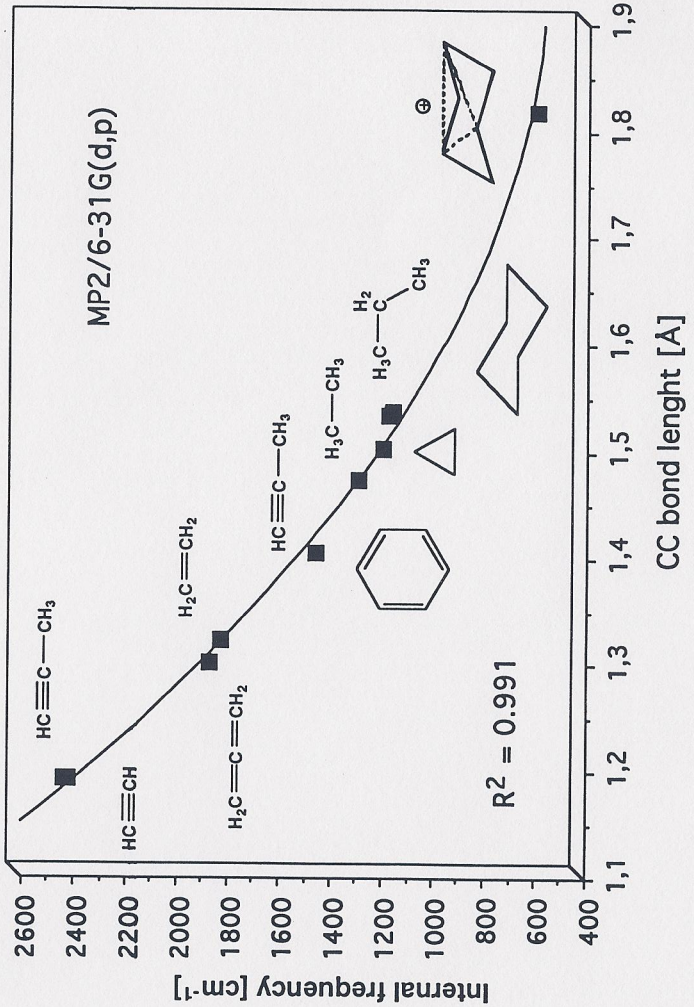

Figure 10. Determination of the C1C3 distance in the trishomotropenylium cation with the help of a quadratic correlation between adiabatic CC stretching frequencies and CC equilibrium bond lengths both calculated at the MP2/6-31G(d,p) level of theory [42].

An adiabatic mode analysis of measured vibrational spectra is possible with a simple perturbation theory approach that was already published in the sixties [44]. The basic equation of vibrational spectroscopy (compare with Eq. 19) can be written in matrix form according to Eq. (74)

$$\mathbf{F}\,\mathbf{D} = \mathbf{G}^{-1}\mathbf{D}\,\underline{\underline{\Lambda}} \tag{74}$$

where the matrix $\underline{\underline{\Lambda}}$ collects the squares of the frequencies ω_μ on its diagonal. Problem (74) can be solved as soon as **F** is known from an appropriate *ab initio* calculation based on the harmonic approximation. One can assume that the calculated normal mode vectors $\mathbf{d}_\mu$ (expressed in terms of internal coordinates and collected in matrix **D**) represent a reasonable approximation to the true normal mode vectors $\mathbf{d}_\mu'$ so that $\mathbf{D} \approx \mathbf{D}'$. This assumption makes some sense in view of the fact that reasonable experimental frequencies can be reproduced from calculated harmonic frequencies by simple scaling procedures. As a matter of fact, all scaling procedures are based on the assumption that **D** is close to the true **D'**.

Once the experimental frequencies are known, it is possible to derive an improved version of Eq. (74) for the experimental situation utilizing the calculated **D**:

$$(\mathbf{F} + \Delta\mathbf{F})\mathbf{D} = \mathbf{G}^{-1}\mathbf{D}\,(\underline{\underline{\Lambda}} + \Delta\underline{\underline{\Lambda}}) \tag{75}$$

in which the correction matrix $\Delta\mathbf{F}$ has to be determined with the help of **F**, **D**, **G** and $\underline{\underline{\Lambda}}$ obtained from the *ab initio* calculation and $\Delta\underline{\underline{\Lambda}}$ from experimental frequencies. This can be done by solving

$$\Delta\mathbf{F}\,\mathbf{D} = \mathbf{G}^{-1}\mathbf{D}\,\Delta\underline{\underline{\Lambda}} \tag{76}$$

For this purpose, one defines the matrices defined in Eqs. (77a) and (78):

$$\tilde{\mathbf{D}} = \mathbf{G}^{-1/2}\,\mathbf{D} \tag{77a}$$

$$\tilde{\mathbf{D}}^{+}\tilde{\mathbf{D}} = \tilde{\mathbf{D}}\,\tilde{\mathbf{D}}^{+} = \mathbf{I} \tag{77b}$$

$$\Delta\tilde{\mathbf{F}} = \mathbf{G}^{1/2}\,\Delta\mathbf{F}\,\mathbf{G}^{1/2} \tag{78}$$

so that the eigenvalue problem (79) can be formulated

$$\Delta\tilde{\mathbf{F}}\tilde{\mathbf{D}} = \tilde{\mathbf{D}}\,\Delta\underline{\underline{\Lambda}} \tag{79}$$

By diagonalization, $\Delta\tilde{\mathbf{F}}$ and $\Delta\mathbf{F}$ can be determined:

$$\Delta\tilde{\mathbf{F}} = \tilde{\mathbf{D}}\,\Delta\underline{\underline{\Lambda}}\,\tilde{\mathbf{D}}^{+} \tag{80a}$$

$$\Delta\mathbf{F} = \mathbf{G}^{-1/2}\,\Delta\tilde{\mathbf{F}}\,\mathbf{G}^{-1/2} \tag{80b}$$

Hence, the experimental situation is described by a change $\Delta\mathbf{F}$ of the force constant matrix and $\Delta\underline{\underline{\Lambda}}$ in the square of the frequencies relative to the calculated force constant matrix and frequencies at some level of *ab initio* theory. Since $\Delta\underline{\underline{\Lambda}}$ is known from the differences between experimental and calculated frequencies, it is straightforward to calculate $\Delta\mathbf{F}$ and the true force constant matrix. Once the true force constant matrix is determined, one can apply the adiabatic mode analysis in the same way as it is applied for calculated vibrational spectra.

As a simple example, experimental and calculated adiabatic mode frequencies of ethene and methane are shown in Figure 11. The two sets of adiabatic frequencies differ on the average by 200 cm^{-1}. It is interesting to compare what one normally considers as the typical CC stretching frequency in ethene (1623 cm^{-1} [45]) and the adiabatic stretching frequency (1566 cm^{-1}, Figure 10). The difference of about 60 cm^{-1} results from coupling of the normal mode dominated by the CC stretching motion with other normal modes and, of course, from some of the assumptions included in the calculation of the experimentally derived adiabatic frequencies.

One can determine experimentally-based adiabatic CC and CH stretching frequencies and correlate them with bond lengths as discussed in the previous section. We have checked the McKean correlations between the isolated CH frequencies and the CH bond lengths in this fashion [42]. Also, we have used experimentally based adiabatic internal CH stretching frequencies to correlate them with other bond properties such as dissociation energies. The existence of correlations between stretching frequencies and dissociation energies has been discussed in the literature [46,47]. The stretching frequency (and its force constant) gives a measure for the curvature of the potential energy surface in the direction of a dissociation reaction. A large (small) stretching frequency suggests a strong (weak) curvature and a large (small) dissociation energy (see Figure 12).

Figure 13 gives the correlation between dissociation energy D_e [48] and adiabatic internal frequency for a number of CH bonds. It can be expressed by Eq. (81)

$$\mathbf{D}_e = (\omega_e - 2080.3)/11.379 \tag{81}$$

where dissociation energies D_e are given in kcal/mol and the correlation coefficient r^2 is 0.969. Clearly, there is a direct relationship between the curvature of the potential energy surface in the direction of the CH bond dissociation and the energy difference between molecule and dissociation products, which can be used to predict D_e values.

These examples confirm that the adiabatic mode analysis can be extended with advantage to experimental vibrational spectra provided all experimental frequencies are known. However, even in the case, in which the set of

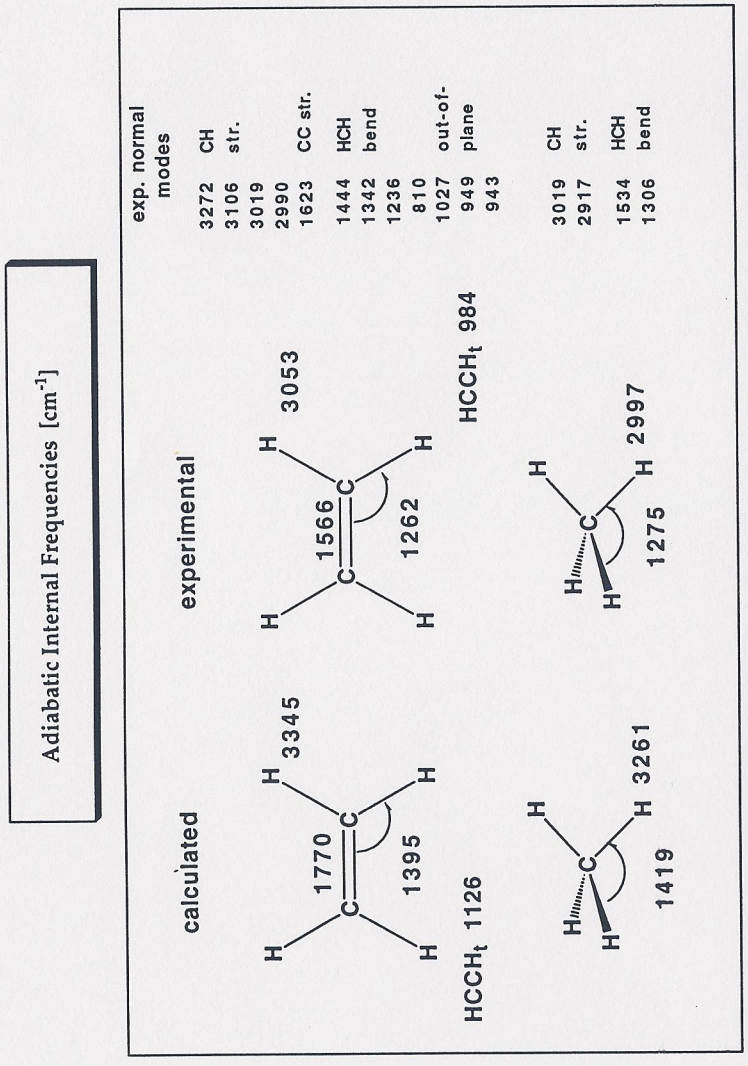

Figure 11. Comparison of directly calculated adiabatic frequencies (HF/6-31G(d,p) calculations) and adiabatic frequencies derived from experimental vibrational frequencies (see text).

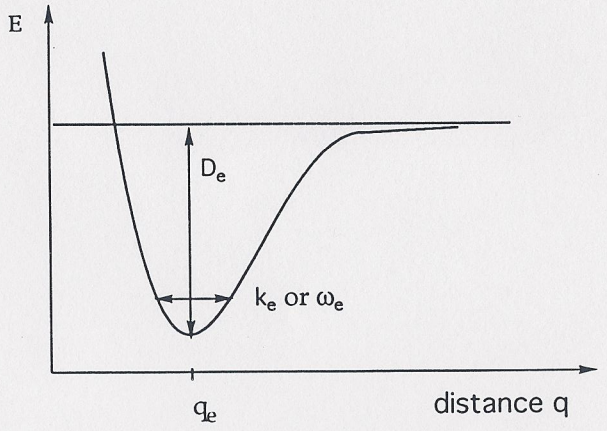

Figure 12. Relationship between dissociation energy and curvature of the potential energy function at the equilibrium represented by force constant k_e or vibrational frequency ω_e.

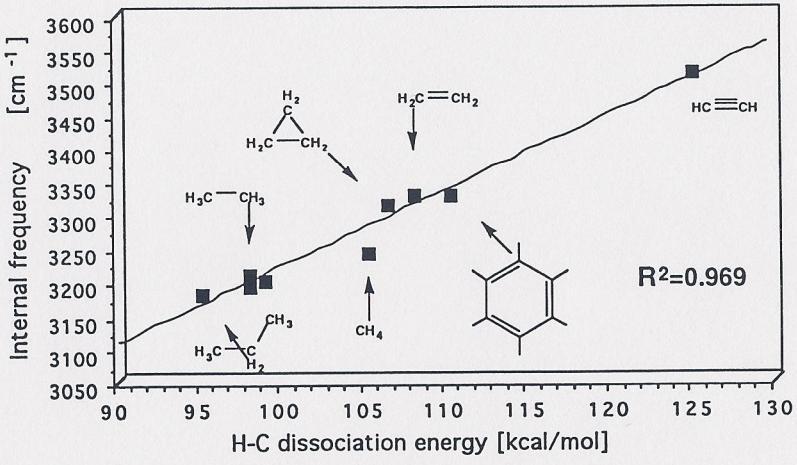

Figure 13. Linear correlation between adiabatic CH stretching frequencies (obtained from experimental frequencies and HF/6-31G(d,p) normal mode vectors) and experimental CH dissociation energies.

experimental frequencies is incomplete, appropriately scaled calculated frequencies can be used to complement the set of experimental frequencies and to carry out the adiabatic mode analysis.

13. A GENERALIZATION OF BADGER'S RULE

Already in the 30s of this century, diatomic molecules were investigated to correlate vibrational spectroscopic constants with bond lengths. The most successful of these relations was the Badger's rule (82) [49]

$$k_e\left(r_e - d_{ij}\right)^3 = C_{ij} \qquad (82a)$$

or

$$r_e = (C_{ij} / k_e)^{1/3} + d_{ij} \qquad (82b)$$

In Eq. (82), r_e is the equilibrium bond length of a diatomic molecule, k_e the associated bond stretching force constant, and C_{ij} as well as d_{ij} are constants, which depend on the rows i and j of the periodic table containing the atoms linked by the bond. Badger's rule has often been used to determine r_e values from spectroscopic constants. Today, it is applied in *ab initio* quantum chemical programs to provide an estimate of the Hessian matrix for the starting point of a geometry optimization, i.e. all distances of the starting geometry are known and appropriate k values have to be estimated to set up the Hessian matrix.

Badger found linear relationships between $k_e^{1/3}$ and r_e in the case of diatomic molecules [49]. Several attempts to generalize these relationships for polyatomic molecules failed because appropriate force constant values k_e for diatomic subunits within a polyatomic molecule were not available. This problem can now be solved with the help of the adiabatic modes. In Figures 14 and 15, $k_e^{1/3}$ versus r_e correlations are shown for the CH and CC adiabatic modes of Figures 7 and 9.

Linear relations (correlation coefficients r^2 for CH: 0.997 and CC: 0.993) are obtained for the diatomic subunits of polyatomic molecules similar to those investigated for diatomic molecules by Badger. This author suggested that the $k_e^{1/3}$ versus r_e relationships for diatomic molecules constituted of atoms from different rows of the periodic table could be reproduced by a series of parallel lines. Badger anticipated similar $k_e^{1/3}$ versus r_e relationships for polyatomic molecules, which can now be checked with the help of adiabatic stretching force constants. In Figure 16, $k_e^{1/3}$-r_e correlations are given for eight different bond types involving H and first row atoms. For all bond types, a linear relationship is obtained with a correlation coefficient $r^2 > 0.98$ or even 0.99. One can distinguish between AH bonds and AB bonds. Within each class correlation lines are parallel or at least almost parallel where Badger's assumption is better fulfilled for the bonds AH with A = C, N, O, and B rather than the AB bonds (Figure 16) [42].

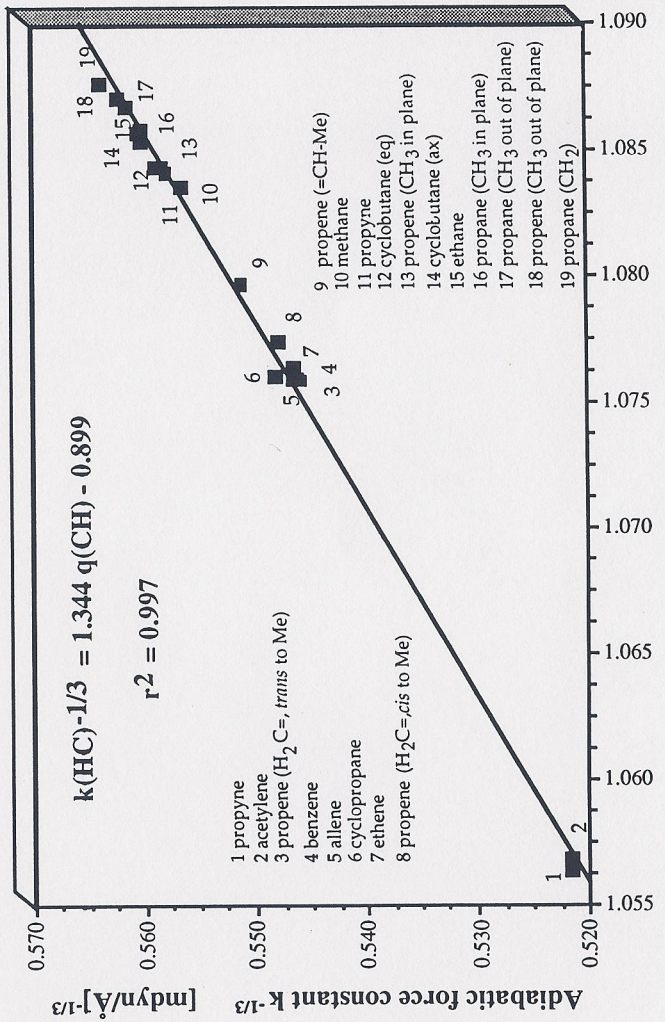

Figure 14. Correlation between adiabatic CH stretching force constants and CH bond lengths according to Badger. (HF/6-31G(d,p) calculations)

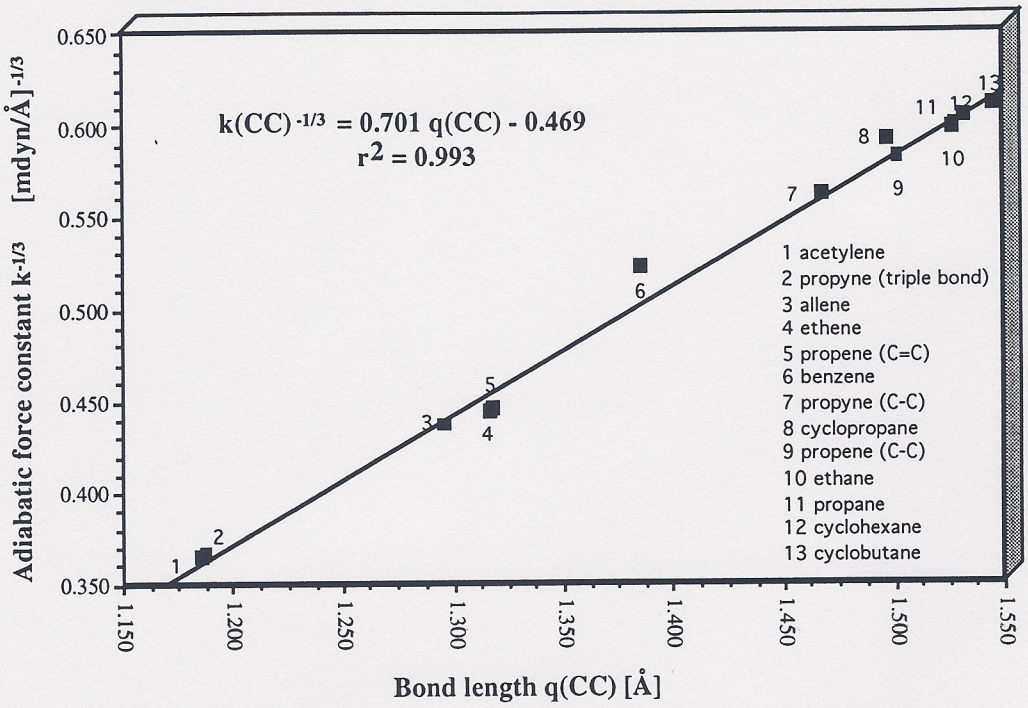

Figure 15. Correlation between adiabatic CC stretching force constants and CC bond lengths according to Badger. (HF/6-31G(d,p) calculations)

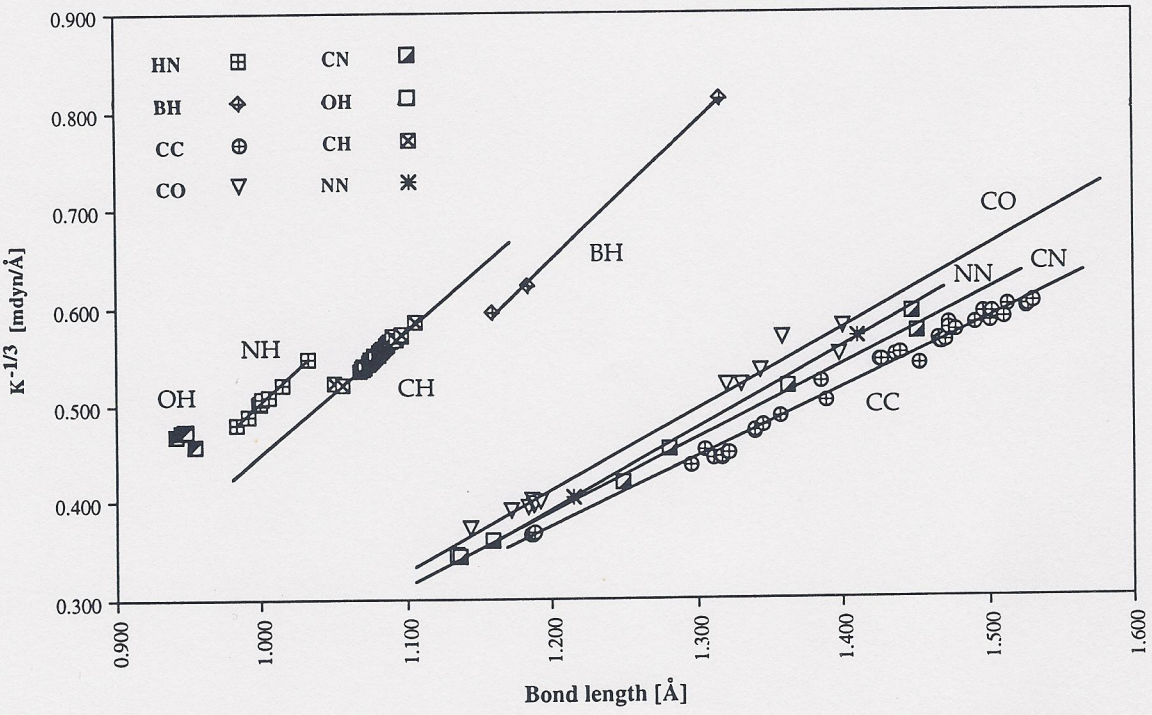

Figure 16. Correlation between adiabatic bond stretching force constants and bond lengths for polyatomic molecules. The correlation lines are parallel for AH bonds and AB bonds as anticipated by Badger. (HF/6-31G(d,p) calculations)

However, Badger's rule is fully confirmed by the adiabatic force constants of polyatomic molecules, which explains its usefulness even for today's research.

14. INTENSITIES OF ADIABATIC INTERNAL MODES

Once internal modes are defined, it is also possible to define the infrared intensity of these modes. For a normal mode, the infrared intensity is calculated with the help of the dipole moment derivatives. The dipole derivatives $\partial\mu/\partial x$ with regard to Cartesian coordinates can be determined in the course of an *ab initio* calculation of vibrational frequencies. The corresponding dipole derivatives with regard to normal coordinates Q_μ are obtained by the transformation

$$\left(\frac{\partial \mu}{\partial Q_\mu}\right) = \left(\frac{\partial \mu}{\partial x}\right) l_\mu \tag{83}$$

where the normal mode vector l_μ relates Cartesian coordinates **x** to the normal coordinate Q_μ according to Eq. (5).

The matrix of dipole derivatives with regard to normal coordinates $\partial\underline{\mu}/\partial Q$ contains the derivatives of the dipole moment components with regard to each normal coordinate. The infrared intensity I_μ of the normal mode l_μ is calculated according to Eq. (84)

$$I_\mu = C \sum_{x=1}^{3}\left(\frac{\partial \mu_x}{\partial Q_\mu}\right)^2 = g_\mu \frac{\pi N_0}{3 c^2} \sum_{x=1}^{3}\left(\frac{\partial \mu_x}{\partial Q_\mu}\right)^2 \tag{84}$$

where C is a conversion factor from atomic units to km/mol that is given by the degeneracy g_μ of normal mode l_μ, the Avogadro number N_0 and the speed of light c.

In a similar way as dipole derivatives with respect to normal coordinates are obtained from dipole derivatives with regard to Cartesian coordinates, one can also obtain dipole derivatives with respect to the internal coordinates associated with the adiabatic internal modes:

$$\left(\frac{\partial \mu}{\partial q_n}\right) = \left(\frac{\partial \mu}{\partial x}\right) a_n \tag{85a}$$

$$\left(\frac{\partial \mu}{\partial q}\right) = \left(\frac{\partial \mu}{\partial x}\right) A \tag{85b}$$

where **A** contains the adiabatic mode vectors $\mathbf{a}_n$ from Eq. (43) and connects the internal coordinates **q** with the Cartesian coordinates **x** by

$$\mathbf{x} = \mathbf{A}\,\mathbf{q} \tag{86}$$

Once adiabatic dipole derivatives are known, the infrared intensity of an adiabatic mode $\mathbf{a}_n$ associated with the internal coordinate q_n is calculated in a similar way as that for a normal mode l_μ:

$$I_n = C \sum_{x=1}^{3}\left(\frac{\partial \mu_x}{\partial q_n}\right)^2 \tag{87}$$

The dipole moment of a bond is given by $\mu = q\,p$, where in this case q is the equilibrium bond length and $\pm p$ defines the partial charges at the atoms connected by the bond. Hence, the derivative of μ with regard to the bond length q should lead to the partial charges p at the atoms linked by the bond, i.e. the infrared intensity of the internal mode should provide a measure for the partial charges of the atoms of a molecule. However, as has been discussed by Zerbi and co-workers [50], one has to consider also the charge flux $\partial p_\alpha/\partial q_n$ toward or away from atom α caused by the stretching of the bond length q_n during a vibration of the bond. If $\partial p_\alpha/\partial q_n < 0$, the flux is directed toward atom α, otherwise away from atom α during a bond stretching vibration that according to the discussion in the previous chapters is best described by $\mathbf{a}_n$. The quantity $\partial p_\alpha/\partial q_n$ measures the deformability of the charge and also provides insight into the electronic nature of the bond in question.

For example, the intensity of an adiabatic CH stretching mode in a hydrocarbon is related to charge p_α and charge flux $\partial p_\alpha/\partial q_n$ according to Eq. (88):

$$I_n(CH) \propto p_H + \frac{\partial p_H}{\partial q(CH)} q(CH) \tag{88}$$

If infrared intensities of bond stretching vibrations are known either from experiment or from theory, atomic charges can be derived. In Table 11, intensity based C and H charges of some simple hydrocarbons are compared with the corresponding Mulliken and virial charges [51]. Also, average intensities per CH bond that have been used by Zerbi to apply Eq. (88) are compared with adiabatic mode intensities. An average intensity per CH bond, e.g., for ethane is obtained by summing the intensities of the three infrared active vibrational modes of ethane and, then, dividing the sum of the intensities by the number of CH bonds in ethane. In Table 11, experimental intensities $l\mu$/CH obtained in this way are listed together with the corresponding calculated values. The latter as well as all other computed values have been obtained at the HF/6-31G(d,p) level of theory while the experimental data are from Zerbi's work [50].

Before the data of Table 11 are shortly discussed, one has to stress that the partial charges derived from adiabatic infrared intensities are not related to Mulliken charges, virial charges or most other atomic charges used in *ab initio* theory. The partial charges p are effective charges which in addition to the atomic monopole contribution, cover the atomic dipole contribution as well. They are

Table 11
Comparison of infrared intensity based, Mulliken, and virial partitioning based partial atomic charges. [a]

Quantity		CH_4	C_2H_6	c-C_3H_6	C_2H_4	C_2H_2	Ref
Intensities [km/mol]							
I_μ/CH, exp.		17.4	28.5	11.5	9.6	35.2	50
I_μ/CH, cal.		9.9	28.7	15.2	15.2	46.0	t.w.
I_n/CH, adiab.		23.4	39.3	20.0	13.3	42.8	t.w.
CH Bond lengths [Å]							
q(CH), cal.		1.0835	1.0858	1.0760	1.0764	1.0568	t.w.
Charges [electron]							
exp. Intensity	C	-0.260	-0.135	-0.170	-0.268	-0.208	50
	H	0.065	0.045	0.085	0.134	0.208	50
adiab. Intensity	C	-0.290	-0.102	-0.187	-0.240	-0.185	t.w.
	H	0.072	0.034	0.094	0.120	0.185	t.w.
Mulliken	C	-0.472	-0.335	-0.261	-0.254	-0.233	28
	H	0.118	0.112	0.130	0.127	0.233	28
virial charges	C	0.244	0.237	0.104	0.082	-0.121	51
	H	-0.061	-0.079	-0.052	-0.041	0.121	51

[a] Calculated values based on HF/6-31G(d,p)//HF/6-31G(d) calculations.

related to those effective charges which have been determined by Zerbi and co-workers [51] from measured intensities. This is confirmed by the fact that the effective charges determined by Zerbi are parallel to the charges based on adiabatic mode intensities (Table 11). Clearly, the average intensity per CH bond is not equal to the adiabatic mode intensity where the differences can be 10-15 km/mol. It is easy to see that an averaging of CH intensities cannot provide reliable intensity values for the determination of atomic charges and that adiabatic mode intensities provide an attractive alternative to average intensities.

It is well known that the electronegativity of a C atom increases with increasing s-character, which is nicely reflected by the virial charges listed in Table 11. The only problem is that virial charges suggest a C^+-H^- bond polarity while Mulliken charges and intensity based charges predict a C^--H^+ bond polarity. The H charges derived from (both experimental and calculated) infrared intensities seem to confirm the increase in the electronegativity of the C atom with increasing s-character. However, the corresponding C charges reveal that the electronegativity change from ethene to acetylene is not correctly described and that a large electronegativity difference between cyclopropane and ethene is predicted. This is not necessarily an indication that the intensity based charges are ill-defined.

As mentioned above, they absorb the effects of (true) atomic charges and atomic dipole moments, where the latter result from the anisotropy of the electron density at an atom. In the virial partitioning method, atomic charges and atomic dipole moments (multipole moments) are separately calculated and their values may cancel largely in the expression for the bond dipole moment. Hence, effective atomic charges and true atomic charges can differ considerably where of course it should be more difficult to discuss effective charges since they contain the cumulative effect of at least two quantities. It is interesting to note that Mulliken charges also do not reproduce the increase in the C electronegativity when going from ethene to acetylene. This might result from an equal splitting of overlap populations to get Mulliken charges, which may mix into the atomic charges higher multipole contributions and, accordingly, may give Mulliken charges the character of effective rather than pure atomic charges.

It is interesting to note that adiabatic intensity based charges in agreement with Mulliken and virial charges suggest similar hybridizations for cyclopropane and ethene as far as the CH hybrid orbitals are concerned. This is in line with other observations, e.g., made for CH dissociation energies. Effective charges derived from average values of experimental intensities fail to describe the close relationship of the CH bonds in ethene and cyclopropane.

We conclude that the adiabatic mode intensities and effective charges derived from them are the localized counterparts of those effective charges derived from measured intensities. They should be more appropriate for the description of the properties of individual bonds. In particular, they should lead to chemically more meaningful effective charges where future work has to show how effective charges, atomic monopole and dipole contributions, and the charge flux are related.

15. INVESTIGATION OF REACTION MECHANISM WITH THE HELP OF THE CNM ANALYSIS

While the adiabatic mode analysis was discussed in the previous sections exclusively for molecules in their equilibrium geometry, we will show in this section that adiabatic vibrational modes are also useful when describing molecules during a chemical reaction. For this purpose, we extend the procedure previously described for constructing adiabatic modes at equilibrium points of the potential energy surface to points along the reaction path [22,23].

The reaction path is defined by the line $\tilde{\mathbf{x}}(s)$ where $\tilde{\mathbf{x}}(s)$ is a column vector of 3K mass-weighted Cartesian coordinates x_i. The reaction path is given parametrically in terms of its arc length s defined by the differential

$$ds^2 = d\mathbf{x}^+\mathbf{M}d\mathbf{x} = d\tilde{\mathbf{x}}^+d\tilde{\mathbf{x}} \tag{89}$$

with M being the diagonal matrix of nuclear masses. The reaction path can be calculated using standard *ab initio* methods and reaction path following algorithms [52]. One starts at the transition state and follows in the forward and backward direction the path downhill to products and reactants, respectively, by evaluating at fixed points along the path gradient and Hessian matrix, which are used to determine at these path points the path direction. It is of advantage to calculate the 3K-L-1 vibrational modes orthogonal to the path direction and use them to describe the reaction valley. This is done by diagonalizing the mass-weighted projected force constant matrix $\tilde{\mathbf{K}}^g(s)$ given by Eq. (90) [53,54]:

$$\tilde{\mathbf{K}}^g(s)\tilde{\mathbf{l}}_\mu{}^g(s) = \omega_\mu^2(s)\tilde{\mathbf{l}}_\mu{}^g(s), \tag{90}$$

where $\tilde{\mathbf{K}}^g(s)$ is defined by Eq. (91).

$$\tilde{\mathbf{K}}^g(s) = (\mathbf{I} - \tilde{\mathbf{P}}(s))\tilde{\mathbf{f}}(s)(\mathbf{I} - \tilde{\mathbf{P}}(s)) \tag{91}$$

In Eq. (91), $\tilde{\mathbf{f}}(s)$ is the mass-weighted Cartesian coordinate force constant matrix, and $\mathbf{I} - \tilde{\mathbf{P}}(s)$ is a projector onto the (3K-L)-1-dimensional subspace of the normal mode vibrations orthogonal to the reaction path mode [53,54]. These modes are called generalized normal modes and describe a "harmonic" reaction valley according to Eq. (92) (compare with Eq. 34).

$$V(s,Q) = V(s) + \frac{1}{2}\sum_{\mu=1}^{N_{vib}} k_\mu{}^g(s)\,[Q_\mu^g(s)]^2 \tag{92}$$

where $k_\mu{}^g(s)$ is the generalized normal mode force constant, $Q_\mu g(s)$ the generalized normal mode coordinate and V(s) the energy profile along the reaction path.

To describe energy transfer along the reaction path, curvature vector K(s), curvature coupling elements $B_{\mu,s}(s)$ and mode-mode coupling elements $B_{\mu,\nu}(s)$ have to be calculated [53,54], of which only the former will be discussed here. The mass-weighted curvature vector $\tilde{\mathbf{K}}(s)$ is defined by (93a) and its Euclidean norm by (93b).

$$\tilde{\mathbf{K}}(s) = \frac{d^2\tilde{\mathbf{x}}(s)}{ds^2} \tag{93a}$$

$$\kappa(s) = \sqrt{\tilde{\mathbf{K}}(s)^+\tilde{\mathbf{K}}(s)} \tag{93b}$$

The curvature coupling elements $B_{\mu,s}(s)$, which represent coefficients of the expansion of the curvature vector in terms of generalized normal modes $\tilde{\mathbf{l}}_\mu{}^g(s)$, are defined by Eq. (94):

$$B_{\mu,s}(s) = \tilde{\mathbf{K}}(s)^+\,\tilde{\mathbf{l}}_\mu{}^g(s); \tag{94}$$

It is common practice to graphically present the norm of the curvature vector, κ(s), and to discuss energy transfer along the reaction path in terms of the maxima of κ(s) [55]. Maximal values of κ(s) indicate those points on the path where energy can flow from the motion along the reaction path into one of the transverse normal vibrational modes or vice versa thus decreasing or increasing the reaction rate. The curvature coupling coefficients $B_{\mu,s}(s)$ of Eq. (94) determine how much energy is transferred into (retrieved from) normal mode $\tilde{\mathbf{l}}_\mu^g(s)$. Due to the delocalized character of normal modes, it is difficult to identify substituents or molecular fragments, which by their vibrations are predominantly responsible for energy transfer from the reaction path mode into vibrational modes (rate reduction) or alternatively can be used to channel external energy *via* vibrational modes into the reaction path mode (rate enhancement). Therefore, it is desirable to express the curvature coupling coefficients $B_{\mu,s}(s)$ of Eq. (94) in terms of vibrational modes that can be directly associated with chemically relevant molecular fragments or structural units. Such modes are the generalized adiabatic internal modes a_n, that can be defined by requiring that the harmonic part of the energy in Eq. (92) has to be minimized with regard to displacements in the (3K-L)-1-dimensional vibrational space (rather than the (3K-L)-dimensional space as originally defined) while relaxing all internal parameters but one [22].

Eq. (95) gives the conditions for obtaining generalized adiabatic internal modes $a_n g(s)$ [22]:

$$V(\mathbf{Q},s) = \min \tag{95a}$$

$$s = \text{const} \tag{95b}$$

$$q_n(s,\mathbf{Q}) = q_n{}^* \tag{95c}$$

where in first order the leading parameter q_n is some linear function of the normal mode coordinates, i.e. in the limit of infinitesimal displacements it is defined by Eq. (96):

$$q_n(s,Q) = \sum_{\mu=1}^{N_{vib}} D_{n\mu}(s) Q_\mu(s) \tag{96}$$

$D_{n\mu}(s)$ denotes an element of a Wilson B-type matrix **D** that connects normal coordinates with internal coordinates. Solving Eq. (95), generalized adiabatic internal modes and related force constants $k_n^a(s)$, mass $m_n^a(s)$, and frequency $\omega_n^a(s)$ are obtained by Eqs. (97) [22],

$$\left(\mathbf{a}_n(s)\right)_\mu = \frac{\dfrac{D_{n\mu}(s)}{k_\mu^g(s)}}{\sum_{\nu=1}^{N_{vib}} \dfrac{D_{n\nu}(s)^2}{k_\nu^g(s)}} \tag{97a}$$

$$k_n^{\,a}(s) = \frac{1}{\sum_{\nu=1}^{N_{vib}} \dfrac{D_{n\nu}(s)^2}{k_\nu^g(s)}} \tag{97b}$$

$$m_n^{\,a}(s) = \frac{1}{G_{nn}(s)} \tag{97c}$$

$$\omega_n^{\,a}(s) = \sqrt{\frac{k_n^{\,a}(s)}{m_n^{\,a}(s)}} \tag{97d}$$

Generalized adiabatic modes can be transformed from normal mode space into Cartesian coordinate space according to Eq. (98)

$$\left(\mathbf{a}_n^g(s)\right)_i = \sum_{\mu=1}^{N_{vib}} (\mathbf{l}_\mu(s))_i \left(\mathbf{a}_n^g(s)\right)_\mu \qquad i = 1,\ldots,3N, \tag{98}$$

where $(\mathbf{l}_\mu)_i$ is component i of normal mode vector $\mathbf{l}_\mu$ in Cartesian coordinates.

Eqs. (97) indicate that there is no difference in applying the adiabatic mode concept to an equilibrium geometry or to a point along a reaction path. In the latter case, the adiabatic modes are defined in a (3K-L)-1- rather than a 3K-L-dimensional space and all adiabatic properties are a function of the reaction coordinate *s*. Obviously, the adiabatic mode concept and the leading parameter principle have their strength in the fact that they can generally be applied to equilibrium geometries as well as any point on the reaction path.

Once generalized adiabatic modes $\mathbf{a}_n^g(s)$ have been defined, the normal modes and curvature vector can be analyzed utilizing the CNM approach of Section 7 [20,21]. For this purpose, the amplitude $A_{n,s}$ is defined [22]

$$A_{n,s} = \frac{\boldsymbol{\kappa}(s)^+ \mathbf{M}(s) \mathbf{a}_n^{\,g}(s)}{\sqrt{\mathbf{a}_n^{g+}(s) \mathbf{M}(s) \mathbf{a}_n^{\,g}(s)}} \tag{99}$$

which characterizes the curvature vector $\boldsymbol{\kappa}(s)$ in terms of generalized adiabatic modes associated with internal coordinates used to describe the reaction system. It corresponds to the A-type amplitude AvAM (with metric **M**, see Eq. 69), which was found to present the best choice for kinetically characterizing normal modes in terms of adiabatic modes in the case of molecules in their equilibrium geometries [20,21]. Eq. (62) ensures that $A_{n,s}$ has the same dimension as $B_{\mu,s}$ and, for $\mathbf{l}_\mu^g = \mathbf{a}_n^g$, amplitude $A_{n,s}$ and coefficient $B_{\mu,s}$ are equal. Both curvature vector and normal modes orthogonal to the reaction path can be characterized in terms of generalized adiabatic internal modes, however for the latter the A-type amplitude AvAF (metric **f**, see Eq. 70) is used since for these modes the dynamic characterization is more important than a kinetic one.

The generalized adiabatic internal modes are essential for the unified reaction valley analysis (URVA) developed by Konkoli, Kraka, and Cremer to investigate reaction mechanisms and reaction dynamics [22,52]. As an example for the application of the generalized adiabatic internal modes, the hydrogenation reaction of the methyl radical is shortly discussed here:

$$CH_3(^2A_2'') + H_2(^1\Sigma_g^+) \rightarrow CH_4(^1A_1) + H(^2S) \tag{100}$$

which has recently been investigated at the MP2/6-31G(d,p) level of theory [22,52]. In Figure 17, the internal coordinates q_n used to describe the reaction complex are given. The most important internal coordinates are q_1 = R1 and q_2 = R2, which describe the length of the breaking HH bond and the length of the CH distance to be formed, respectively. The calculated dependence of the normal mode frequencies $\omega_\mu(s)$ in dependence of *s* is shown in Figure 18. The latter reveals that the strongest changes in the mode frequencies are observed for modes #11 and #8, which accordingly should closely be connected with the bond breaking/bond forming process of reaction (100). Noteworthy is an avoided crossing point at s = -0.3 $amu^{1/2}$ Bohr involving the a_1-symmetrical modes #11 and #8 (notation 11/8) and a reaction path bifurcation point at s = 0.4 $amu^{1/2}$ Bohr that leads to zero and, then, imaginary values of the frequencies of the 1e-symmetrical modes #1 and #2 (see Figure 18).

In Figure 19a, the reaction path curvature $\kappa(s)$ is shown as a function of the reaction coordinate *s*. There are two distinct peaks of $\kappa(s)$ in the transition state (TS; the location of the TS is defined by *s* = 0) region at s = -0.1 and 0.7 $amu^{1/2}$ Bohr (peaks $\kappa 2$ and $\kappa 3$), which are associated with the normal modes 11/8 (i.e. #11 before and #8 after the avoided crossing at s = -0.3) and to some smaller extend with modes #5 and 8/11 as the decomposition of $\kappa(s)$ in terms of normal mode contributions reveals. If energy is stored in mode 11/8, it will be channelled into the reaction path mode and lead to rate acceleration. Dissipation of energy into mode 8/11 is small since the avoided crossing between modes #11 and #8 at s =

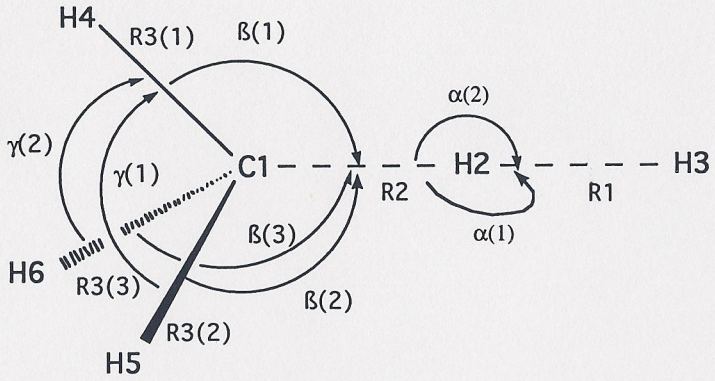

Figure 17. Internal coordinates used to describe the reaction complex of the hydrogenation reaction $CH_3(^2A_2'')+ H_2(^1\Sigma_g^+)$ -> $CH_4(^1A_1) + H(^2S)$.

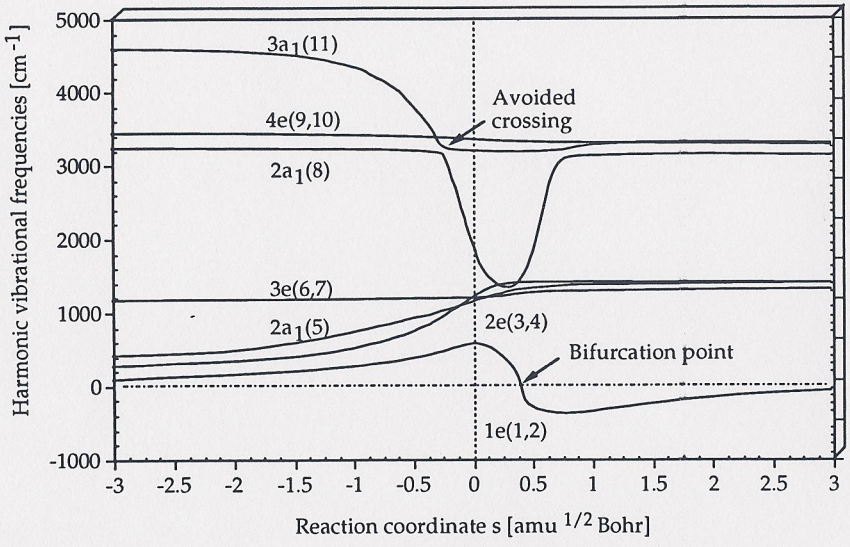

Figure 18. Representation of normal mode frequencies $\omega_\mu(s)$ along the reaction path. Symmetry symbols and numbering of normal modes are given according to the order of normal modes calculated for the reactants. The position of the transition state corresponds to s = 0 $amu^{1/2}$ Bohr and is given by a vertical line. The value $\omega_{1e}(s) = 0$ indicates the location of a bifurcation point (s = 0.4 $amu^{1/2}$Bohr) of the reaction path. Imaginary 1e frequencies calculated for s > 0.4 $amu^{1/2}$ Bohr are given as negative numbers.

-0.3 $amu^{1/2}$ Bohr is strongly localized and, therefore, the exchange of energy rather limited.

In the case of reaction (100), it is easy to determine the nature of modes #11 (HH bond stretching) and #8 (CH bond stretching) and, in this way, to relate the peaks of the curvature vector with the corresponding changes in electronic structure. However, in general this way of analysis is difficult and, therefore, a decomposition of the curvature vector in terms of generalized adiabatic internal modes gives a chemically more meaningful insight into the nature of the reaction path curvature as can be seen from Figure 19b.

The analysis of the reaction path curvature in terms of generalized adiabatic modes reveals that peak κ2 close to the TS is strongly dominated by the R1 adiabatic HH stretching mode led by internal coordinate R1 while peak κ3 after the TS results from the adiabatic CH stretching mode led by internal coordinate R2. Since the motions associated with R1 and R2 are closely related in the reaction, each of the two peaks κ2 and κ3 also depends to some smaller degree on the adiabatic partner mode of the pair R1-R2. This duality is indicative for the fact that HH bond breaking and CH bond forming are closely connected in the reaction. When the R1-peak of κ(s) (peak κ2) starts to develop the HH bonds begins to break and the CH bond to be formed (Figure 19b). The positive R1-contribution to κ2 is accompanied by a negative, but much smaller R2 contribution, which can be interpreted as indication that the reaction system resists a further decrease in R2 needed for the formation of the CH bond.

From the second to the third curvature maximum at s = 0.6 $amu^{1/2}$ Bohr (peak κ3) the R2 and R1 amplitudes $A_{n,s}$ exchange their role, i.e. the R2 amplitude becomes dominant and positive while the R1 amplitude is relatively small and negative. Peak κ3 identifies the point where the CH bond forming process is basically finished if the reaction $CH_3 + H_2$ is considered; for the reverse reaction CH_4 +H, it is the point where bond C1H2 starts to be broken accompanied by the resistance of the electronic structure to form as a new bond the HH bond associated with R1.

If one investigates the changes in κ(s) (Figure 19b), a clear picture of the mechanism of the HH bond breaking and CH bond forming process emerges: These processes occur simultaneously in the region of the curvature peaks κ2 and κ3 (-0.1 s < 0.6) as indicated by maxima or minima of the amplitudes associated with the internal parameters R1 and R2 describing HH and CH bond. Hence, the generalized adiabatic modes help to understand the mechanism of bond breaking and bond forming and, therefore, they are essential for UVAR [22]. Their real value becomes obvious when investigating larger reaction systems. For example, the application of UVAR to the Diels-Alder reaction between ethene and butadiene implies an analysis of reaction path direction and reaction path curvature in terms of 42 normal modes, which represents a rather complicated and chemically complex task difficult to interpret [53]. However, use of generalized adiabatic modes directly clarifies, which structural changes determine direction and curvature of the reaction path [53].

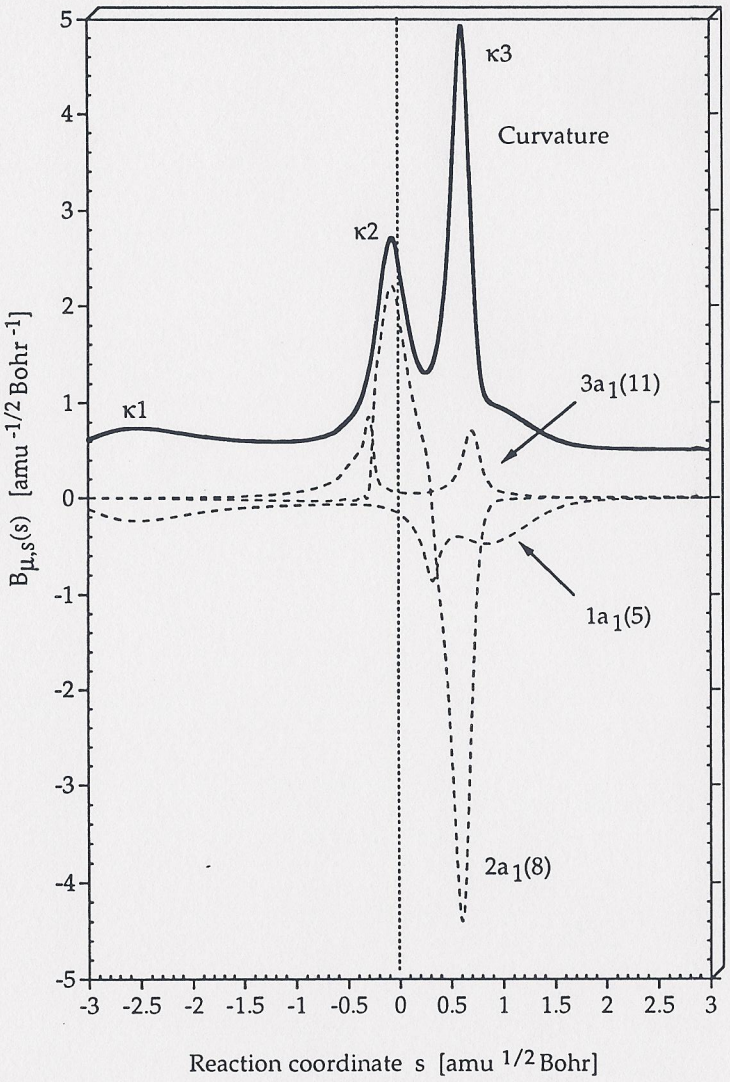

Figure 19a. Characterization of the reaction path curvature κ(s) (thick solid line) in terms of normal mode-curvature coupling coefficients $B_{\mu,s}(s)$ (dashed lines). The curve κ(s) has been shifted by 0.5 units to more positive values to facilitate the distinction between κ(s) and $B_{\mu,s}(s)$. For a definition of the internal coordinates, compare with Figure 17. The position of the transition state corresponds to s = 0 amu$^{1/2}$ Bohr and is indicated by a vertical line.

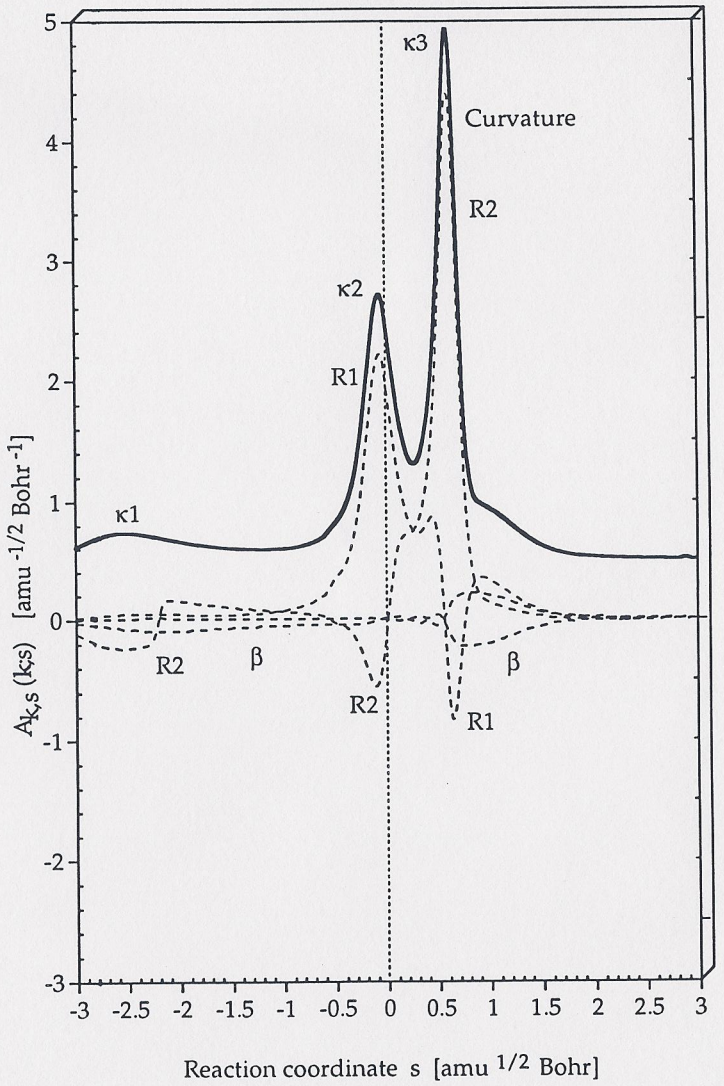

Figure 19b. Characterization of the reaction path curvature κ(s) (thick solid line) in terms of adiabatic mode-curvature coupling amplitudes $A_{n,s}(s)$ (dashed lines). The curve κ(s) has been shifted by 0.5 units to more positive values to facilitate the distinction between κ(s) and $A_{n,s}(s)$. For a definition of the internal coordinates, compare with Figure 17. The position of the transition state corresponds to s = 0 amu$^{1/2}$ Bohr and is indicated by a vertical line.

16. CONCLUSIONS

One of the major goals of vibrational spectroscopy is to associate measured frequencies with structural features of a molecule and, thereby, to facilitate its identification. These efforts have led to a number of rules that concern the similarity and transferability of force constants and frequencies from one molecule to another provided they contain similar structural units [1-9]. To provide a mathematical basis for the comparison of measured vibrational frequencies and force constants, the adiabatic internal vibrational modes were defined [18], which enable one to investigate molecular fragments in terms of their internal vibrations defined by the pair $(q_n, \mathbf{v}_n)$.

The derivation of the adiabatic vectors has been motivated by the observation that the masses of the atoms of a molecule effectively hinder the appearance of localized internal vibrations $\mathbf{v}_n$ associated with fragments ϕ_n. However, localized internal vibrations $\mathbf{v}_n$ can be obtained by setting the generalized momenta associated with those internal parameters not used for the description of fragment ϕ_n to zero and solving the Euler-Lagrange equations under this condition. This approach is equivalent to exciting the internal motion $\mathbf{v}_n$ by a constant perturbation q_n^* of the leading parameter associated with ϕ_n and, then, relaxing the distortions of all other internal coordinates q_m until a minimum of the energy is obtained.

Once adiabatic internal modes $\mathbf{a}_n$ are defined (see Section 5), it is straightforward to derive an appropriate adiabatic force constant k_n, an adiabatic mass m_n, and an adiabatic mode frequency ω_n (see Section 6). The choice of m_n as an appropriate fragment mass is confirmed by the fact that it represents a generalized reduced mass $1/G_{nn}$. Furthermore, it guarantees that a fragment frequency does not depend on the masses of those atoms that do not belong to ϕ_n and, therefore, it is typical of ϕ_n and its properties. The dynamics of a vibrating molecular fragment ϕ_n is uniquely characterized by the internal frequency ω_n, the internal mass m_n, and the internal force constant k_n and this makes it possible to compare different molecular fragments of one or many polyatomic molecules in a systematic way.

There are immediately a number of applications of adiabatic internal modes that lead to a new dimension in the analysis of vibrational spectra. For example, the adiabatic vectors $\mathbf{a}_n$ are perfectly suited to present a set of localized internal modes that can be used to analyze delocalized normal modes. This has led to the CNM analysis (Sections 7 and 8) of calculated vibrational spectra of molecules as was discussed in Section 9. With the CNM analysis it is rather easy to correlate the vibrational spectra of different molecules (Section 10). With the help of perturbation theory and calculated normal modes, the determination of adiabatic modes and the CNM analysis can be extended to experimental spectra (Section 12).

Once adiabatic modes are known either from calculations or experimental data, adiabatic frequencies can be used to characterize chemical bonds. For example, it is easy to verify a McKean relationship [30] between adiabatic CH or CC stretching frequencies and the corresponding bond lengths (Section 11). It can

be shown that with the adiabatic force constants k_n Badger's rule can be extended from diatomic to polyatomic molecules (Section 13). In addition, it is possible to determine adiabatic mode intensities, which can be utilized to derive effective charges for the atoms of a molecule (Section 14). Most important, generalized adiabatic vibrational modes can be defined for reacting molecules so that a detailed analysis of the direction and the curvature of the reaction path becomes possible. This is the basis of the UVAR approach [22,23], which leads to a detailed analysis of mechanism and dynamics of chemical reactions (Section 15). A chemically easy to understand description of energy transfer and energy dissipation, quantum mechanical tunneling, structural and electronic changes, etc. occurring along the reaction path can be made, which provides new and very detailed insights into chemical reactions.

ACKNOWLEDGEMENT

This work was supported by the Swedish Natural Science Research Council (NFR). All calculations were done on a CRAY YMP/416 and C94 of the Nationellt Superdatorcentrum (NSC), Linköping, Sweden. The authors thank the NSC for a generous allotment of computer time. Useful comments by Zoran Konkoli are appreciated.

REFERENCES

1. E.B.J. Wilson, J.C. Decius, and P.C. Cross, Molecular Vibrations, The Theory of Infrared and Raman Vibrational Spectra, McGraw-Hill, London, 1955.
2. G. Herzberg, Infrared and Raman Spectra of Polyatomic Molecules, Van Nostrand, New York, 1945.
3. P. Gans, Vibrating Molecules, Chapman and Hall, London, 1971.
4. L.A. Woodward, Introduction to the Theory of Molecular Vibrations and Vibrational Spectroscopy , Clarendon Press, Oxford, 1972.
5. S. Califano, Vibrational States, Wiley, New York, 1976.
6. D.A. Long, Raman Spectroscopy, McGraw-Hill, London, 1977.
7. K. Nakanishi, and P.H. Solomon, Infrared Absorption Spectroscopy, Holden-Day, San Francisco, 1977.
8. N.B. Colthup, L.N. Daly, and S.E. Wilberley, Introduction to Infrared and Raman Spectroscopy, Academic Press, New York, 1990.
9. J.M. Hollas, High Resolution Spectroscopy, Butterworths, London, 1982.
10. P. Pulay, in *Ab initio* Methods in Quantum Chemistry, Part II, K.P. Lawley (ed.), Wiley, New York, 1987, p. 241.
11. B.A. Hess and L.J. Schaad, Chem Rev., 86 (1986) 709.
12. J. Gauss and D. Cremer, Adv. Quant. Chem., 23 (1992) 205.
13. L. Andrews and M. Moskovits (eds.), Chemistry and Physics of Matrix-Isolated Species, North-Holland, Amsterdam, 1989.
14. W. Sander, Angew. Chem., Int. Ed. Engl., 29 (1989) 344.

15. (a) A. Patyk, W. Sander, J. Gauss, and D. Cremer, Angew. Chem., 101 (1989) 920. (b) A. Patyk, W. Sander, J. Gauss, and D. Cremer, Chem. Ber., 123, (1990) 89.
16. (a) W. Sander, G. Bucher, F. Reichel, and D. Cremer, J. Am. Chem. Soc., 113 (1991) 5311. (b) M. Trommer, W. Sander, C.-H. Ottosson, and D. Cremer, Angew. Chem., 107 (1995) 999 .
17 (a) S. Wierlacher, W. Sander, C. Marquardt, E. Kraka, and D. Cremer, Chem. Phys. Lett., 222 (1994) 319. (b) R. Albers, W. Sander, H. Ottosson and D. Cremer, Chem. Eur. J., 2 (1996) 967.
18. Z. Konkoli and D. Cremer, Int. J. Quant. Chem., submitted.
19. Z. Konkoli, J.A. Larsson, and D. Cremer, Int. J. Quant. Chem., submitted.
20. Z. Konkoli and D. Cremer, Int. J. Quant. Chem., submitted.
21. Z. Konkoli, J.A. Larsson, and D. Cremer, Int. J. Quant. Chem., submitted.
22. Z. Konkoli, E. Kraka, and D. Cremer, J. Phys. Chem., in press.
23. Z. Konkoli, E. Kraka, and D. Cremer, J. Comp. Chem., in press.
24. (a) N. Neto, Chemical Physics, 91 (1984) 89; 101. (b) N. Neto, Chemical Physics, 87 (1984) 43.
25. Y. Morino and K. Kuchitsu, J. Chem. Phys., 20 (1952) 1809.
26. P. Pulay and F. Török, Acta Chim. Hung., 47 (1966) 273.
27. G. Keresztury and G. Jalsovszky, J. Mol. Structure, 10 (1971) 304.
28 D. Cremer, E. Kraka and K.J. Szabo, in: The Chemistry of Functional Groups, The Chemistry of the Cyclopropyl Group, Vol 2, Z. Rapport (ed), J. Wiley, Ldt., New York, 1995, p.43.
29 (a) D. F. McMillen and D. M. Golden, Am. Rev. Phys. Chem., 33 (1982) 493. (b) M. H. Baghal-Vayjooee and S. Benson, J. Am. Chem. Soc., 101 (1979) 2840. (c) W. Tsang, J. Am. Chem. Soc., 107 (1985) 2872.
30. (a) D.C. McKean, Chem. Soc. Rev., 7 (1978) 399. (b) D.C. McKean, Int. J. Chem. Kinet., 71 (1984) 445.
31. S.-J. Kim, H.F. Schaefer, E. Kraka and D. Cremer, Mol. Phys., 88 (1996) 93.
32. E. Kraka, D. Cremer, J. Fowler, and H.F. Schaefer, J. Am. Chem. Soc. 118 (1996) 10595.
33. B. Casper, D. Christen, H.-G. Mack, H. Oberhammer, G. A. Argiiello, B. Jülicher, M. Krönberg, and H. Willner, J. Phys. Chem., 100 (1996) 3983.
34. (a) K. C. Nicolaou and W. M. Dai, Angew. Chem. Int. Ed. Engl., 30 (1991) 1387. (b) K. C. Nicolaou and A. L. Smith, Acc. Chem. Res., 25 (1992) 497.
35. (a) R. Gleiter and D. Kratz Angew. Chem., 105 (1993) 884. (b) P. Chen, Angew. Chem., 108 (1996) 1584.
36. Kraka, E. and D. Cremer, Chem. Phys. Lett., 216 (1993) 333.
37. Kraka, E. and D. Cremer, J. Am. Chem. Soc., 116 (1994) 4929.
38. R. Marquardt, W. Sander, and E. Kraka, Angew. Chem. Int. Ed. Engl., 35 (1996) 746.
39. R. Marquardt, W. Sander, E. Kraka, and D. Cremer, Angew. Chem., submitted.
40. (a) G. Bucher, W. Sander, E. Kraka, and D. Cremer Angew. Chem. Int. Ed Engl., 31 (1992) 1230. (b) E. Kraka, D. Cremer, G. Bucher, and W. Sander, Chem. Phys. Lett., in press. (c) W. Sander, G. Bucher, H. Wandel, A. Kuhn, E. Kraka, and D. Cremer, J. Am. Chem. Soc., submitted.
41. E. Kraka, J.A. Larsson, and D. Cremer, J. Phys. Chem., to be published.
42. J.A. Larsson and D. Cremer, to be published.
43. K. J. Szabo, E. Kraka, and D. Cremer, J. Org. Chem., 61 (1996) 2783.
44. See, e.g., the discussion in Ref. 3.
45. For a collection of experimental frequencies, see W.J. Hehre, L. Radom, P.v.R. Schleyer, and J.A. Pople, Ab Initio Molecular Orbital Theory, Wiley, New York, 1986.
46. A.A. Zavitsas, J. Phys. Chem., 91 (1987) 5573.
47. D.J.Swanton, and B.R. Henry, J. Chem. Phys., 86 (1987) 4801.
48. Handbook of Chemistry and Physics, 64th edition, Weast, 1984.
49. (a) R.M. Badger, J. Chem. Phys., 2 (1934) 128. (b) R.M. Badger, J. Chem. Phys., 3 (1935) 552. (c) R.M. Badger, Phys. Rev., 48 (1935) 284.
50. (a) C. Castiglioni, M. Gussoni and G. Zerbi, J. Mol. Struct., 141 (1986) 341. (b) M. Gussoni, C. Castiglioni and G. Zerbi, J. Mol. Struct. THEOCHEM, 138 (1986) 203. (c) M. Gussoni, C. Castiglioni, M. N. Ramos, M. Rui and G. Zerbi, J. Mol. Struct., 224, (1990) 445 and references cited therein.
51. (a) R. F. W Bader and T. T. Nguyen-Dang, Adv. Quantum Chem., 14 (1981) 63. (b) R. F. W. Bader, T. T. Nguyen-Dang and Y. Tal, Rep. Prog. Phys., 44 (1981) 893. (c) R. F. W. Bader, Atoms in Molecules - A Quantum Theory, Oxford University Press, Oxford, 1990. (d) R. F. W. Bader, P. L. A. Popelier and T. A. Keith, Angew. Chem., 106 (1994) 647
52. For a recent review, see E. Kraka in Encyclopedia of Computational Chemistry, H.F. Schaefer III (ed.), Wiley, submitted.
53. W.H. Miller, N.C. Handy, and J.E. Adams, J. Chem. Phys., 72 (1980) 99.
54. M. Page and J.W.J. McIver, J. Chem. Phys., 88 (1988) 922.
55. S. Kato and K. Morokuma, Chem. Phys., 73 (1980) 3900.
56. T. Johnsson, Z. Konkoli, E. Kraka, and D. Cremer, to be published.